REPORT DOCUMENTATION PAGE

Form Approved
OMB NO. 0704-0188

1. AGENCY USE ONLY (Leave Blank)	2. REPORT DATE	3. REPORT TYPE AND DATES COVERED
	March 2010	M.S. Thesis; 9/2004 - 3/2010

4. TITLE AND SUBTITLE
Preignition and Autoignition Behavior of the Xylene Isomers

5. FUNDING NUMBERS
DAAD19-03-1-0070
W911NF-07-1-0522

6. AUTHOR(S)
Robert H. Natelson

7. PERFORMING ORGANIZATION NAME(S) AND ADDRESS(ES)
Drexel University, 3141 Chestnut Street, Philadelphia, PA 19104

8. PERFORMING ORGANIZATION REPORT NUMBER

9. SPONSORING / MONITORING AGENCY NAME(S) AND ADDRESS(ES)
U. S. Army Research Office
P.O. Box 12211
Research Triangle Park, NC 27709-2211

10. SPONSORING / MONITORING AGENCY REPORT NUMBER

11. SUPPLEMENTARY NOTES
The views, opinions and/or findings contained in this report are those of the author(s) and should not be construed as an official Department of the Army position, policy or decision, unless so designated by other documentation.

12 a. DISTRIBUTION / AVAILABILITY STATEMENT	12 b. DISTRIBUTION CODE
Approved for public release; distribution unlimited.	

13. ABSTRACT (Maximum 200 words)

The relative preignition and autoignition reactivity of o-, m- and p-xylene has been studied. Preignition experiments were conducted in a pressurized flow reactor facility at 600-850 K temperatures, 8 atm pressure, and lean equivalence ratios. Analysis of the data included carbon monoxide and carbon dioxide measurements using a nondispersive infrared analyzer and molecular oxygen measurements using an electrochemical oxygen cell. Identification of intermediate species was performed using gas chromatography with flame ionization detection and a mass spectrometer. Additional experiments were conducted in a single cylinder research engine. Neat o- and m-xylene were oxidized in the reactor under preignition conditions. They showed no reactivity, so mixtures of each isomer with n-dodecane were tested and compared, and intermediate species were identified. This data helped resolve a recent controversy regarding the relative reactivity of the xylene isomers. To study the autoignition of the xylenes, the isomers neat, in binary mixtures with n-decane, and in six-component JP-8 surrogates were tested in the single cylinder research engine. The experimental data were analyzed and compared to existing chemical kinetic models, and it was concluded that at lower temperatures (<850 K), the xylenes show similar reactivity, and at higher temperatures, o-xylene is the more reactive isomer.

14. SUBJECT TERMS	15. NUMBER OF PAGES
Xylene; autoignition; JP-8; flow reactor.	95
	16. PRICE CODE

17. SECURITY CLASSIFICATION OR REPORT	18. SECURITY CLASSIFICATION ON THIS PAGE	19. SECURITY CLASSIFICATION OF ABSTRACT	20. LIMITATION OF ABSTRACT
UNCLASSIFIED	UNCLASSIFIED	UNCLASSIFIED	U

NSN 7540-01-280-5500

Standard Form 298 (Rev.2-89)
Prescribed by ANSI Std. 239-18
298-102

Enclosure 1

Preignition and Autoignition Behavior of the Xylene Isomers

A Thesis

Submitted to the Faculty

of

Drexel University

by

Robert Harris Natelson

in partial fulfillment of the

requirements for the degree

of

Master of Science in Mechanical Engineering

March 2010

DEDICATIONS

This work is dedicated to the past graduate students of the Combustion Chemistry research group, whose work over the last three decades in the Hess Lab has made the present study possible.

ACKNOWLEDGMENTS

I would first like to thank my advisors Dr. Nicholas P. Cernansky and Dr. David L. Miller for providing me the opportunity to conduct my graduate research studies. They have been patient as I have steadily improved in my experimental and theoretical abilities under their guidance. I would also like to thank Dr. Vedha Nayagam at NASA Glenn Research Center for first introducing me to the research area of combustion.

My colleague at Hess Lab, Matthew Kurman, has been an invaluable collaborator in my work, and I cannot imagine completing this study without his support in the laboratory. I would also like to acknowledge the thoughtful discussions I have had with my other Hess Lab friends, including Jamie Lane, Ashutosh Gupta, Rodney Johnson, David Lenhert, Xiaohui Gong, Jincai Zheng, Seuk Chun Choi, Yi Ma, Kevin Wujcik, and Brian Folkes.

I would also like to thank my other friends especially Hanita Lessen and my parents and sister for bearing with me while I worked on this study.

This material is based upon work supported by the U.S. Army Research Office under Grant Nos. DAAD19-03-1-0070 and W911NF-07-1-0522 and by the U.S. Air Force Office of Scientific Research under Grant No. FA9550-08-1-0040 (AFRL Energy IPT).

Table of Contents

LIST OF TABLES

LIST OF FIGURES

ABSTRACT

Preignition and Autoignition Behavior of the Xylene Isomers

Robert H. Natelson

Nicholas P. Cernansky, Ph.D. and David L. Miller, Ph.D.

The relative preignition and autoignition reactivity of the xylene isomers (*o*-, *m*- and *p*-xylene, or 1,2-, 1,3-, and 1,4-dimethylbenzene) has been studied. The principal objectives were to determine the relative reactivity among the isomers and the key oxidation branching pathways. Preignition experiments were conducted in a pressurized flow reactor facility at 600-850 K temperatures, 8 atm pressure, and lean equivalence ratios. Online analysis of the data included carbon monoxide and carbon dioxide measurements using a nondispersive infrared analyzer and molecular oxygen measurements using an electrochemical oxygen cell. Offline analysis, for identification and quantification of intermediate species, was performed using gas chromatography with flame ionization detection and coupling to a mass spectrometer. Additional experiments were conducted in a single cylinder research engine.

Neat *o*- and *m*-xylene were oxidized in the PFR under preignition conditions. They showed no reactivity, so mixtures of each isomer with *n*-dodecane were tested and compared, and intermediate species were identified. This data helped resolve a recent controversy regarding the relative reactivity of the xylene isomers. Additionally, a mixture of *p*-xylene / *n*-dodecane was studied. To study the autoignition of the xylenes, the isomers neat, in binary mixtures with *n*-decane, and in six-component JP-8 surrogates were tested in the single cylinder research engine. The experimental data were analyzed and compared to existing chemical kinetic models, and it was concluded that at lower

temperatures (<850 K), the xylenes show similar reactivity, and at higher temperatures, *o*-xylene is the more reactive isomer. The data can be used for the improvement of xylene chemical kinetic models, and the conclusions from this study will aid in the selection of the appropriate xylene isomer for JP-8 surrogate fuels.

CHAPTER 1. INTRODUCTION

1.1 Motivation

The United States Department of Defense Directive 4140.43 mandated JP-8 as the universal military fuel (U.S. Army TACOM, 2001). JP-8 is a kerosene fuel similar to international commercial jet fuel Jet A-1 except for the addition of three additives – a fuel system icing inhibitor, a corrosion inhibitor, and a static dissipater additive. The consequences of using JP-8 throughout all power systems including compression ignition (CI) engines include possible issues (e.g., ignition timing, power output, fuel flexibility, fuel economy, and emissions) arising with the behavior of the fuel at the preignition and autoignition conditions in the 600-1000 K temperature range. Furthermore, applications of combustion knowledge at this temperature regime may increase because of the development of advanced CI engines operating at lower temperatures (< 2000 K), designed to reduce particulate matter (soot) and nitrogen oxide and nitrogen dioxide (NO_x) emissions (Akihama *et al.*, 2001; Sjöberg and Dec, 2007; Dec, 2009). To stabilize autoignition at these lower temperatures may require control of two-stage ignition. The chemistry of combustion relevant for two-stage ignition is a complex process involving multiple competing temperature- and pressure-dependent reaction pathways and characterized by phenomena such as cool flames and Negative Temperature Coefficient (NTC) behavior.

For the prediction of fuel behavior under current engine combustion conditions and for the development of future, advanced engines, the ideal solution would be testing real fuels in the engines at representative experimental conditions. However, this is

impossible for a number of reasons. Real fuels such as JP-8 contain hundreds of components, with varying composition. For JP-8, the varying composition arises because the specifications are broad to allow for easier, economical production. Select specifications are shown in Table 1-1 and illustrate that JP-8 is defined by general chemical properties and distillation points. Exact chemical composition is not specified; rather, general limits are applied, such as the maximum of 25.0% aromatics by volume. Even with average fuels of known composition, it is difficult to explain their ignition behavior in engine experiments considering the complexity of chemistry coupled with fluid mechanics and heat transfer. Furthermore, the task of testing fuels in current engines requires substantial commitments of time and money, and when considering new designs, the investment to physically construct prototypes can be excessive.

Table 1-1: JP-8 specifications defined by MIL-DTL-83133E.

Property	**Minimum**	**Maximum**
Aromatics	-	25.0% vol
Alkenes	-	5.0% vol
Naphthalenes	-	3.0% vol
Total sulfur	-	0.30% mass
Distillation – 10% recovered	-	205°C
Evaporation point	-	300°C
Flash point	38°C	-
API gravity	37.0	51.0
Freezing point	-	-47°C
Heat of combustion	42.8 MJ/kg	-
Hydrogen content	13.4% mass	-
Fuel system icing inhibitor	0.10% vol	0.15% vol

An alternative to physical testing is the simulation of combustion in engines. Once the engine parameters (e.g., engine geometry, valve timing, and fuel rail pressure),

either current or future, are defined, the combustion of the fuel can be evaluated if the chemical kinetics (CK) and computational fluid dynamics (CFD) can describe the combustion behavior and transport. However, the large number of components in real fuels is the limiting factor toward describing real fuel combustion with detailed CK. Therefore, there is a recognized need in the combustion community for the development of surrogates, mixtures of a small number of components at known proportions that mimic the composition and behavior of real fuels such as gasoline, diesel, and jet fuels (Colket *et al.*, 2007 & 2008; Farrell *et al.*, 2007; Pitz *et al.*, 2007). Once a surrogate fuel has been tested and verified and its CK model developed, this surrogate fuel CK model can be coupled with CFD for the evaluation of fuel combustion.

In early surrogate research, Sarofim and coworkers at the University of Utah developed a mixture to match the composition and distillation properties of JP-8 (Violi *et al.*, 2002). This surrogate was composed of 30% *n*-dodecane, 20% *n*-tetradecane, 20% methylcyclohexane, 15% *m*-xylene (1,3-dimethylbenzene), 10% *iso*-octane (2,2,4-trimethylpentane), and 5% tetralin (1,2,3,4-tetrahydronaphthalene) by volume. Figure 1-1 shows the structure of the components. In a non-premixed counterflow flame study by Egolfopoulos and coworkers at the University of Southern California, this surrogate was tested and compared to average samples of JP-8 and Jet-A jet fuel, POSF-3773 and POSF-4658[1], respectively (Holley *et al.*, 2007). Experiments were conducted to test for ignition and extinction limits. The surrogate ignited more easily and was more resistant to extinction than either average jet fuel sample.

[1] The referencing system for all JP-8 and Jet-A samples in this paper are those used by Wright-Patterson Air Force Base.

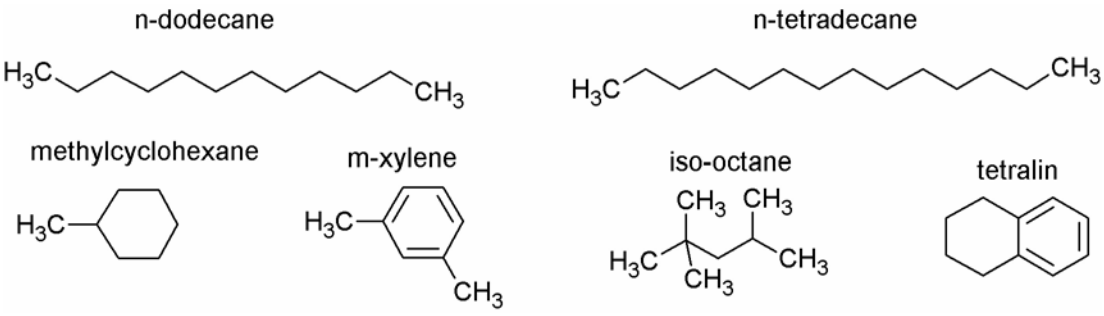

Figure 1-1: Components of the Violi *et al.* (2002) JP-8 surrogate.

However, in a separate non-premixed counterflow flame configuration at the University of California, San Diego, a six-component surrogate of 30% *n*-dodecane, 20% *n*-tetradecane, 20% methylcyclohexane, 15% *o*-xylene (1,2-dimethylbenzene), 10% *iso*-octane, and 5% tetralin by volume was tested (Seshadri, 2006). Figure 1-2 shows the structure of the xylene isomers. Experiments measured autoignition and extinction limits and the researchers compared the surrogate to JP-8 POSF-4177. The surrogate matched extinction characteristics of this JP-8 sample well, but auto ignited more easily.

It is important to note that by using different samples of JP-8 these research groups made an unfortunate assumption that all JP-8's react similarly. In previous work using two JP-8 samples in the pressurized flow reactor (PFR) of the current study it was observed that JP-8 POSF-3773 was much more reactive than JP-8 POSF-4177[2] under preignition conditions (Lenhert *et al.*, 2007). Preignition reactivity in the PFR has been shown to match high temperature behavior in the counterflow flame experiments (Colket *et al.*, 2007). Therefore, assuming POSF-4177 and POSF-3773 provided a "standard" to compare reactivity was flawed.

[2] For additional information on these jet fuel samples, see Section 3.4.

While the comparison to JP-8's of different reactivity may be questionable, direct comparison of the autoignition and extinction results of Holley *et al.* (2007) and Seshadri (2006) reveal interesting phenomena regarding the behavior of the xylene isomers in mixtures. This observation that the surrogate was more reactive with *m*-xylene than with *o*-xylene contradicted the previous understanding of xylenes. Past work comparing reactivity of neat xylenes concluded that *o*-xylene was more reactive than *m*-xylene (Lovell *et al.*, 1934; Jackson, 1951; Wright, 1960; Emdee *et al.*, 1990 & 1991; Roubaud *et al.*, 2000a). The importance of resolving this issue is because the xylene isomers, as key high-octane number antiknock fuels, constitute a major component of real fuels. For example, a sample of California reformulated gasoline contained 7.09% *m*-xylene and 2.27% *o*-xylene by mass, commercial diesel fuel contains approximately 9.20% alkylbenzenes by mass, and commercial jet fuel contains approximately 13.40% simple aromatics by mass (Guibet, 1999). Moreover, understanding the behavior of the xylenes, individually and in blends, is likely to be an essential step in understanding the behavior of larger and more complex aromatics that are also found in appreciable amounts in real fuels.

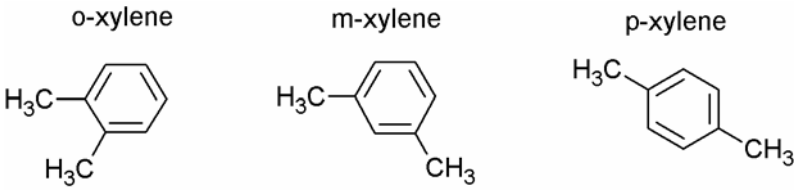

Figure 1-2: The three xylene (dimethylbenzene) isomers.

1.2 Objectives

The first objective of this study was to determine the relative reactivity of the xylene isomers at preignition and autoignition conditions, neat and in surrogate mixtures. This aids in the selection of the appropriate xylene isomer if xylene is considered for a surrogate fuel. The second objective was to isolate the key branching pathways for the xylene isomers at preignition and autoignition conditions. This provides the experimental work necessary for the development of xylene CK models. The mechanistic analysis extends to lower temperatures (<900 K) and stoichiometries (<0.5) than past xylene experimental and modeling work, which concentrated on temperatures greater than 900 K and equivalence ratios closer to stoichiometric.

1.3 Approach

To study the preignition behavior of the xylenes, a series of experiments was conducted in the PFR. First, the neat xylenes were tested in the PFR. They were not reactive neat, so they were mixed with a more reactive species to initiate the radical pool, a method that has previously been used to study other non-reactive species (Agosta *et al.*, 2004). As an alternative to the complexity of the six-component Violi *et al.* (2002) surrogate, each xylene isomer was mixed in binary blends with a more reactive species, *n*-dodecane, which has been studied in detail by Lenhert (2004a). In the low temperature regime of hydrocarbon combustion, a key indicator of reactivity is the production of carbon monoxide (CO), which does not oxidize to carbon dioxide (CO_2) at a significant rate at these conditions (Wilk *et al.*, 1989). These experiments ascertained the relative reactivity of the xylenes, neat and in mixtures, at preignition conditions. Additional

experiments were conducted in a single cylinder research engine. In the research engine, the key reactivity indicator is the in-cylinder pressure rise as a function of the crankshaft position. The xylenes were tested neat and in mixtures to determine the relative reactivity of the isomers at autoignition conditions.

To determine the key branching pathways of the xylenes at preignition conditions, a suite of chemical analytic instruments were utilized. For the measurement of CO and CO_2, a non-dispersive infrared analyzer was used online in the PFR facility. An electrochemical oxygen cell was used online for measuring O_2. A gas chromatograph (GC) with a flame ionization detector (FID) and coupled to a mass spectrometer (MS) was utilized for the identification of key stable intermediates produced from the xylenes oxidized in the PFR. Mechanistic analysis, the process of elucidating chemical kinetic pathways based on intermediate speciation, was conducted. To aid in the data interpretation, past xylene work was reviewed. Additionally, xylene models in the literature were analyzed at the conditions of the PFR. Results were studied with rate-of-production analyses to determine the key branching pathways of xylene oxidation according to the published models.

CHAPTER 2. BACKGROUND

2.1 Hydrocarbon Oxidation Chemistry

The theory of gas-phase combustion of hydrocarbons was developed by Semenov (1935). The concentration history of radicals, species with an unpaired electron in the outer valence shell and thus highly reactive, controls the overall reaction rate. Chemical reactions are categorized into propagation, branching, and termination reactions, based on how they change the radical population. In propagation reactions, the number of radical products is the same as the number of radical reactants. In branching reactions, there are more radical products; in termination reactions, there are fewer radical products. Because certain radicals are produced from specific reactions, which are primarily dependent upon temperature, the hydrocarbon combustion phenomena is separated into several temperature regions. The low and intermediate temperature regions, separated by the NTC phenomena, occur from approximately 500-1000 K, and the high temperature region occurs above 1000 K (Westbrook and Dryer, 1984). The low temperature region is controlled by alkylperoxy radicals ($R\dot{O}_2$), the intermediate temperature region is controlled by hydroperoxy ($H\dot{O}_2$) and hydroxyl radicals ($\dot{O}H$), and the high temperature region is controlled by hydroxyl, oxygen ($\dot{O}$), and hydrogen ($\dot{H}$) radicals. The temperature limits shift with pressure; at higher pressure the transitions occur at higher temperatures. Through extensive experimental testing and kinetic modeling, the general scheme of hydrocarbon combustion for linear alkanes of carbon numbers 3 and

higher has been developed and well-accepted (Griffiths, 1995; Miller *et al.*, 2005; Battin-Leclerc, 2008).

Figure 2-1 shows a schematic of reaction pathways for the oxidation of linear alkanes at low and intermediate temperatures. Initially, hydrogen is abstracted from a parent fuel molecule, RH, to produce an alkyl radical, $\dot{R}$. Molecular oxygen addition to the alkyl radical produces an alkylperoxy radical, $R\dot{O}_2$. The alkylperoxy radical has a number of different possible pathways, including reactions to produce an alkyl radical and carbon monoxide, or an alkoxy radical, $R\dot{O}$, and a hydroxyl radical, or two alkoxy radicals and molecular oxygen, or two alkoxy radicals, or isomerization to produce an alkylhydroperoxy radical, $\dot{Q}OOH$. This latter reaction is reversible, and is increasingly likely with molecules of higher carbon number. If the temperature is high enough, $\dot{Q}OOH$ may decompose by β-scission[3] to produce an alkene, $R = R$, and $H\dot{O}_2$, or an alkene, an aldehyde, $RCHO$, and a hydroxyl radical, $\dot{O}H$, or it can undergo β-scission and subsequent molecular oxygen addition and further decomposition to ultimately yield an aldehyde, hydroperoxy and alkyl radicals, and carbon monoxide, or it can react with O_2 to produce a peroxyalkylhydroperoxy radical, $\dot{O}OQOOH$. Subsequent isomerization of the peroxyalkylhydroperoxy radical produces an alkyldihydroperoxy radical, $HOO\dot{R}OOH$, which then decomposes to produce a ketohydroperoxide, $OROOH$, and $\dot{O}H$. Further decomposition of the

[3] β-scission is the breaking of the carbon-carbon bond at the carbon atom one removed from the radical site (Law, 2006).

ketohydroperoxide produces another hydroxyl radical, an alkanoyl radical, $\dot{R}O$, and an aldehyde. The production and decomposition of the alkyldihydroperoxy radical is thus a key pathway for first-stage ignition, as two hydroxyl radicals are produced. However, as some of the reversible steps are exothermic at higher temperatures, they may revert to the formation of an alkyl radical and O_2 from an alkylperoxy radical. This produces the NTC region, where overall reactivity of the fuel decreases because fewer radicals, particularly hydroxyl radicals, are produced. The alkyl radical can decompose by β-scission to produce a smaller alkyl radical and an alkene. If the temperature increases to approximately 900 K, the intermediate temperature region reactions become important, and the alkyl radical reacts with O_2 to produce a hydroperoxy radical and an alkene.

Reaction of $H\dot{O}_2$ with a parent fuel molecule produces hydrogen peroxide, H_2O_2, and an alkyl radical. The decomposition of hydrogen peroxide, when the temperature is high enough for high temperature reactions, produces two hydroxyl radicals. This is a trigger of second-stage ignition. The hydroxyl radicals then react with fuel molecules to produce alkyl radicals and H_2O, which, with the corresponding liberation of heat, drives the high temperature combustion of the fuel.

The reactivity of the fuel, as monitored by CO production, at these temperatures is shown in Figure 2-2. In the low temperature region, as temperature increases, reactivity increases and CO is produced from the decomposition of species such as alkoxy and alkanoyl radicals. When the temperature increases enough, CO production decreases because in the NTC region, $R\dot{O}_2$ is decomposing to $\dot{R}$ and O_2. The alkyl radicals are then decomposing without reacting with oxygen.

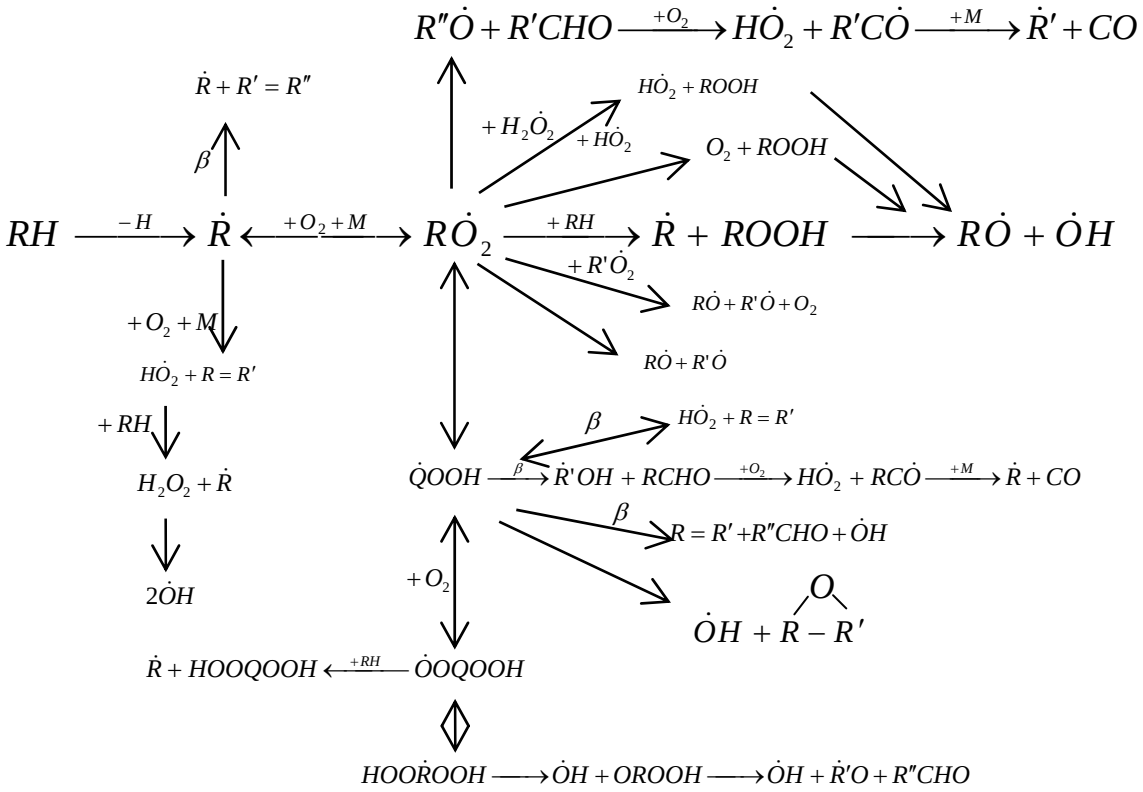

Figure 2-1: Schematic of oxidation of linear alkane hydrocarbons, C_{3+}.

The oxidation of aromatic hydrocarbons does not completely follow the pathways of Figure 2-1. Brezinsky (1986) and Simmie (2003) reviewed the work on the oxidation of aromatics such as benzene, toluene, ethylbenzene, and 1-methylnaphthalene. At temperatures as low as 600 K, reactivity of these aromatics is possible, producing peroxy species similar to the low temperature alkane pathways. At higher temperatures, the benzene ring can break to form smaller species such as alkenes and dienes.

A major focus in aromatic hydrocarbon combustion is research on soot formation. Aromatic rings are a key precursor in soot formation theories. As such, the formation and further reaction of aromatics similar to xylene are a major research topic. Richter and Howard (1999) and McEnally *et al.* (2006) reviewed the work on the formation of polyaromatic hydrocarbons (PAH) from smaller species. Propargyl and cyclopentadienyl

radicals and acetylene, Figure 2-3, are key species with double and triple bonds that are precursors to the resonance exhibited in aromatics, and lead to the formation of aromatic rings. The rings nucleate to form larger species and eventually soot. The complex phenomenon is mainly a high temperature process, but nevertheless a key motivation for research in aromatic hydrocarbon oxidation chemistry. As such, the conclusions of this study, including the selection of a xylene isomer surrogate component, may have implications on which aromatic species to study for soot formation.

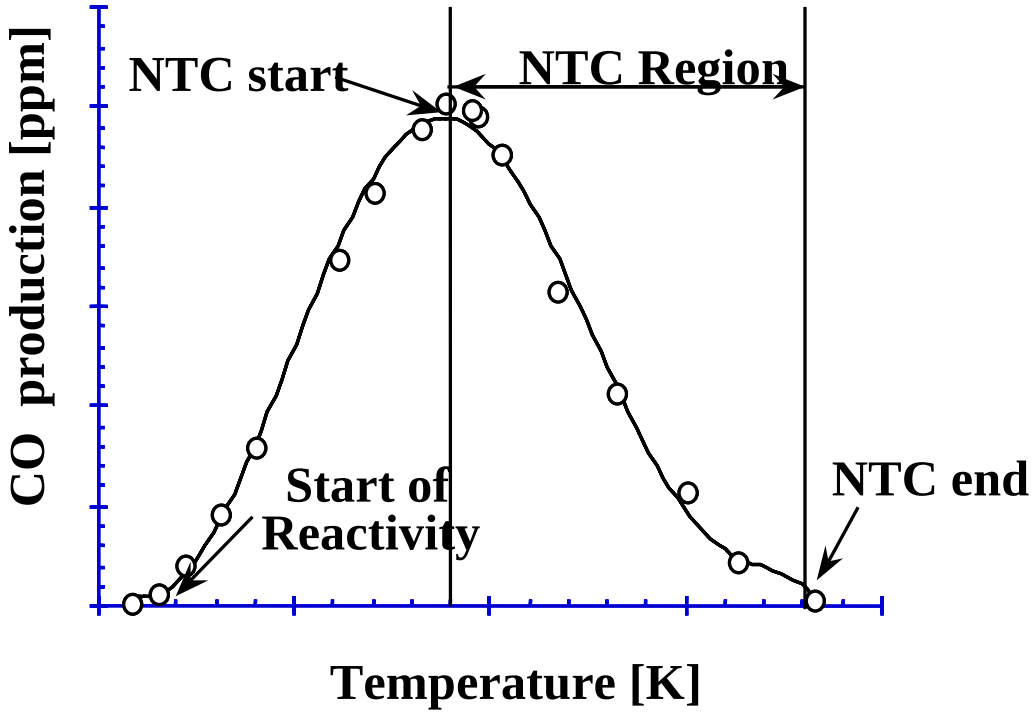

Figure 2-2: CO as an indicator of reactivity at low temperatures.

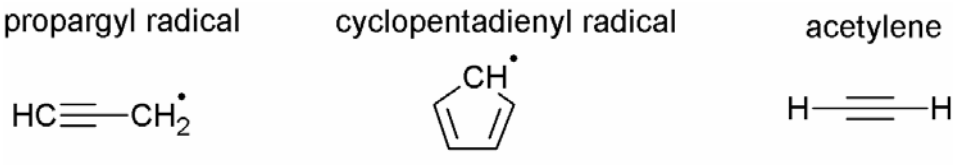

Figure 2-3: Key soot formation precursors.

2.2 Previous Xylene Combustion Work

A number of studies over the years have compared the autoignition characteristics of the xylene isomers. In a single cylinder engine, the critical compression ratio (CR), the lowest CR at which knock occurs, was measured and it was found that the order from lowest to highest at 600 RPM (revolutions per minute) was *o*-xylene (9.6), *m*-xylene (13.6), and *p*-xylene (14.2) (Lovell *et al.*, 1934). When compression ratio is lower, the in-cylinder pressure is lower, and therefore the in-cylinder temperature is lower; it requires a more reactive species to ignite at a lower compression ratio. The same ordering was found in measuring spontaneous ignition temperatures, with *o*-xylene igniting at a much lower temperature (734 K) than either *m*-xylene (836 K) or *p*-xylene (838 K) (Jackson, 1951). In another study, the oxidation of the xylene isomers was investigated in a sub-atmospheric quartz vessel (Wright, 1960). *o*-Xylene was the most reactive isomer, with an activation energy for the oxidation process of 38 kcal/mol, 1 and 2 kcal/mol less than *m*- and *p*-xylene, respectively. The slow oxidation of *m*-xylene and *p*-xylene was also compared at temperatures of 733-785 K in a static reactor and the behavior of the isomers was found to be nearly identical (Barnard and Sankey, 1968a). A separate study under the same conditions explored the oxidation of *o*-xylene; this isomer was much more reactive than the former two (Barnard and Sankey, 1968b). *o*-Xylene oxide (1,3-dihydro-2-benzofuran, or phthalan), Figure 2-4, was the key intermediate

identified in the partial oxidation of o-xylene in a flow reactor (Loftus and Satterfield, 1965). More recently, using time-resolved UV absorption at 265 nm, measurements were conducted on the production of *p*-methyl-benzyl radicals, Figure 2-5, produced by *p*-xylene oxidation at temperatures of 1050-1400 K behind reflected shock waves in a shock tube (Eng *et al.*, 1998). Additionally, exhaust samples were collected and analyzed with GC/MS from the combustion of the xylene isomers in a single cylinder engine operating at 1500 RPM (Gregory *et al.*, 1999). Key intermediates were toluene, benzene, styrene, and ethyltoluene, Figure 2-6.

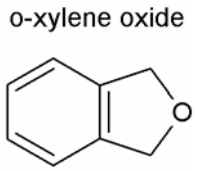

Figure 2-4: Key o-xylene intermediate identified by Loftus and Satterfield (1965).

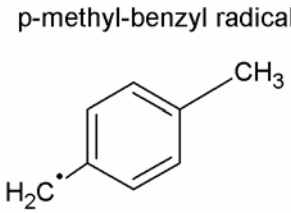

Figure 2-5: Key p-xylene radical intermediate measured by Eng *et al.* (1998).

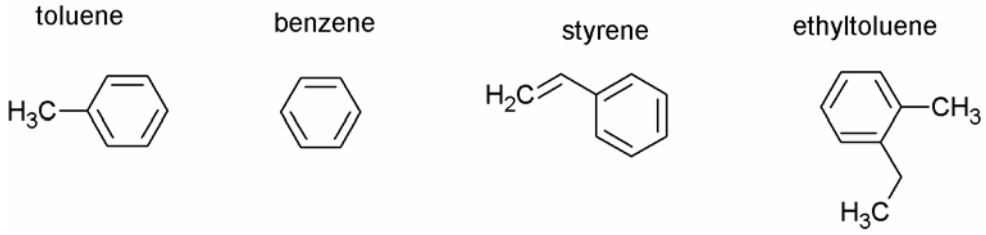

Figure 2-6: Key xylene intermediates identified from engine exhaust sampling by Gregory *et al.* (1999). Each ethyltoluene isomer was identified from its respective xylene isomer.

Species produced during *m*-xylene and *p*-xylene oxidation were measured in an atmospheric flow reactor at temperatures of 1093-1199 K and equivalence ratios of 0.47-1.7 at Princeton University (Emdee *et al.*, 1991). The major aromatic intermediates identified were benzene, toluene, methyl-benzaldehyde (tolualdehyde), ethyltoluene, benzaldehyde, ethylbenzene, styrene, methyl-benzyl alcohol, methylstyrene, and 1,2-ditolylethane, Figure 2-7. The major aliphatic intermediates were methane, acetylene, ethene, cyclopentadiene, and vinylacetylene. It was estimated from simulation analysis that abstraction of a side-chain H to form the methylbenzyl (xylyl) radical accounted for 65-75% of the fuel consumption. It was also predicted that abstraction of a methyl group to produce toluene accounted for 20-30% of the fuel consumption. Oxidation of *p*-xylene took place through both sequential and simultaneous oxidation of the methyl side chains. Overall, the behavior of the isomers was similar - though with *p*-xylene slightly more reactive than *m*-xylene - except for the formation of *p*-xylylene from *p*-xylene oxidation, which did not have an analogous pathway in *m*-xylene oxidation. Another study in the same experimental facility explored the oxidation of *o*-xylene at 1155 K temperature and equivalence ratios from 0.69-1.7 (Emdee *et al.*, 1990). *o*-Xylene exhibited greater reactivity than *m*- or *p*-xylene. The key pathway leading to the higher reactivity of *o*-xylene was determined to be the formation of *o*-xylylene during simultaneous oxidation of the side chains. *o*-Xylylene isomerizes to form styrene, which then produces phenyl and vinyl radicals, Figure 2-8. Alternatively, a sequential oxidation route was considered, which produces *o*-tolualdehyde. Measurement of substantial quantities of *o*-tolualdehyde indicated its importance.

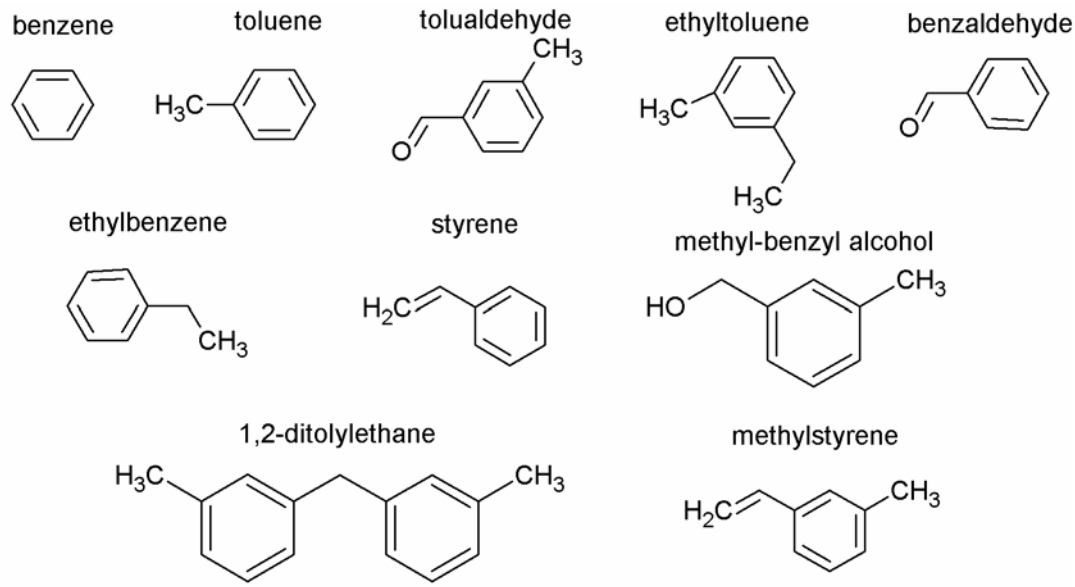

Figure 2-7: Aromatic intermediates identified from high temperature *m*- and *p*-xylene oxidation by Emdee *et al.* (1991). Tolualdehyde, ethyltoluene, methyl-benzyl alcohol, and methylstyrene isomers were identified from their respective parent fuel isomers.

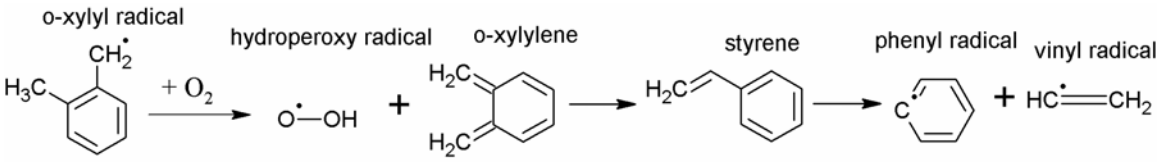

Figure 2-8: Key branching pathway for *o*-xylene identified by Emdee *et al.* (1990).

A study at the Lille University of Science and Technology compared the behavior of the xylenes from low to intermediate temperatures (Roubaud *et al.*, 2000a). The three isomers were oxidized neat in a rapid compression machine (RCM) at temperatures of 600-900 K, pressures of 5-15 atm, and an equivalence ratio of 1.0. *o*-Xylene exhibited much different oxidation behavior from *m*-xylene and *p*-xylene, in that *o*-xylene showed NTC behavior similar to *n*-alkanes while *m*-xylene and *p*-xylene did not exhibit NTC reactivity, resembling the oxidation of toluene. The minimum temperatures for autoignition were 679 K for *o*-xylene (at 12 atm), 906 K for *m*-xylene (at 21 atm), and

904 K for *p*-xylene (at 22 atm). It was concluded that in general the two factors deciding low temperature reactivity of alkylbenzenes are the proximity and length of the alkyl chains. A follow-up study explored the low temperature branching pathways of *o*-xylene in the RCM using GC, MS, and FID (Roubaud *et al.*, 2000b). Twenty-two species were identified. Species accounting for the highest concentration of carbon atoms were 2-hydroxybenzaldehyde, 2-methylbenzaldehyde (*o*-tolualdehyde), and *o*-xylene oxide, Figure 2-9. The pathway leading to these stable intermediates is similar to low temperature oxidation of *n*-alkanes: hydrogen abstraction, followed by molecular oxygen addition, followed by isomerization to produce alkylhydroperoxy radicals, followed by decomposition producing the stable intermediates.

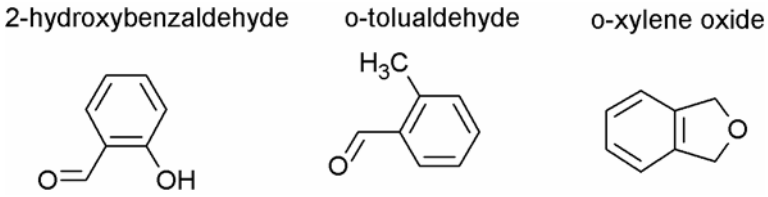

Figure 2-9: Key species identified from *o*-xylene oxidation by Roubaud *et al.* (2000b).

The oxidation of *p*-xylene was recently studied at the French National Centre for Scientific Research (CNRS) in an atmospheric pressure jet-stirred reactor at temperatures of 900-1300 K and equivalence ratios of 0.5-1.5, with detailed intermediate speciation and quantification conducted with GC/MS/FID (Gaïl and Dagaut, 2005). Key aromatic intermediates were benzaldehyde, toluene, benzene, cyclopentadiene, styrene, and methylethylbenzene. Another study in the same facility explored *m*-xylene oxidation (Gaïl and Dagaut, 2007). Results were overall similar, but indicated that *m*-xylene reacts

slightly slower than *p*-xylene. A third study in the facility explored *o*-xylene oxidation (Gaïl *et al*., 2008). *o*-Xylene exhibited greater reactivity than the other isomers at similar conditions. At higher temperatures, the oxidation of the xylenes has been studied in oxygen / argon mixtures in a shock tube (Battin-Leclerc *et al.*, 2006). At temperatures of 1330-1800 K, pressures of 6.7-9 atm, and equivalence ratios of 0.5-2, the ignition delay times were similar for all of the isomers.

CHAPTER 3. EXPERIMENTAL SETUP

3.1 Pressurized Flow Reactor Facility

The preignition experiments were conducted in the PFR facility at Drexel University. The PFR is a plug flow reactor designed to study the chemistry of hydrocarbon combustion with relative isolation from the effects of fluid mechanics and heat transfer (Koert and Cernansky, 1992). The PFR was originally designed and constructed by Koert (1990), which includes all design details. Updates to the facility have been added and recorded since 1990, such as a method for calculating mixture inlet temperatures (Ramotowski, 1992) and the installations of a 3-kW heater (Wang, 1999), a high-pressure fuel syringe pump (Agosta, 2002), a Windows-based computer for data acquisition with an upgraded LabVIEW program (Lenhert, 2004b), and updated air circulation and bead heaters (Kurman, 2009). The main features of the facility, shown in Figure 3-1, and the operational methodology will now be described.

To perform an experiment, nitrogen and oxygen are mixed to form a synthetic air free of contaminants. This synthetic air is heated to the reaction temperature with 10-kW and 3-kW heaters. Liquid fuel from the syringe pump is injected into the centerline of a heated nitrogen stream one meter from the reactor inlet to ensure complete vaporization and mixing. The synthetic air and the prevaporized fuel/nitrogen mixture are rapidly mixed in an opposed jet annular mixing nozzle at the entrance of the quartz reactor tube, which is within the pressure vessel of the PFR. The nitrogen dilution of the fuel limits temperature rise due to heat release. In order to promote temperature uniformity, the walls of the pressure vessel are heated by nine independently controlled 800-W bead

heaters. Temperature rise is monitored by comparing experimental sample temperatures with calculated inlet temperatures; average temperature rise for these experiments was 40 K.

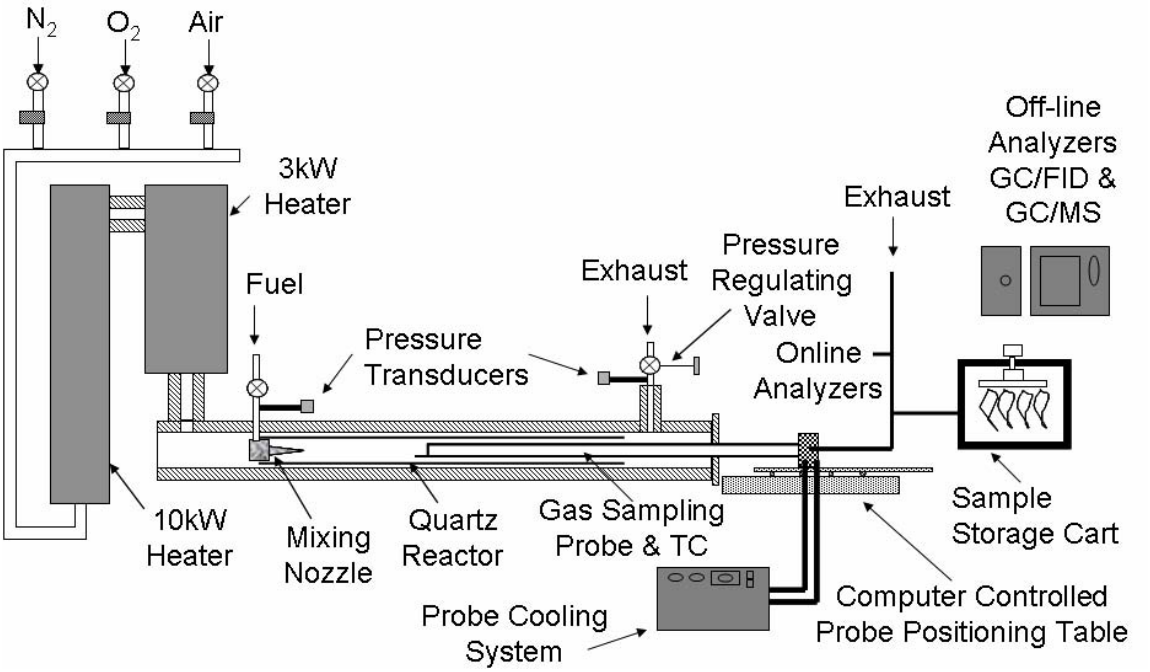

Figure 3-1: Schematic of the PFR.

A water-cooled, glass-lined stainless steel probe extracts samples from the centerline of the quartz reactor tube and quenches the chemical reactions. Sample temperatures are measured using a type-K thermocouple integrated into the probe assembly. For each experiment in this study, a controlled cool down (CCD) methodology was followed so that the PFR was operated over a range of temperatures at a constant residence time and pressure. Measurements during the CCD allow creation of a "reactivity map" of the fuel. An experiment was started at the maximum temperature,

and then the heaters were shut off and the reactor cooled at a rate of 2-5 K/min. Because decreasing temperature caused the density of the gas mixture to increase, the probe position was adjusted inward to maintain a constant residence time. The extracted gas samples continuously flowed through a heated sample line to a non-dispersive infrared (NDIR) analyzer for carbon monoxide (CO) and carbon dioxide (CO_2) measurements. Instrumental uncertainty is ± 50 ppm for CO and ± 100 ppm for CO_2.

All experiments were conducted at fuel-lean conditions, such that the equivalence ratio $\phi < 1$. This is done because, for practical reasons, reducing the equivalence ratio reduces the temperature rise due to heat release and reduces the undesired possibility of the mixture undergoing hot ignition, and for application reasons, since future advanced CI engines may operate at lean conditions. The equivalence ratio is traditionally defined as the ratio of the actual fuel / oxidizer mixture to the stoichiometric fuel / oxidizer mixture. Specifically, Eq. 3-1 gives

$$\phi = \frac{x + \frac{y}{4}}{a + \frac{z}{2}} \tag{3-1}$$

The values *x*, *y*, and *z* refer to the amounts of carbon, hydrogen, and oxygen in the fuel, according to Eq. 3-2

$$C_x H_y O_z + a*(O_2 + 3.76N_2) \rightarrow xCO_2 + \frac{y}{2} H_2O + 3.76aN_2 \tag{3-2}$$

For these experiments, ϕ is selected and the molecular formula of the selected fuel (*x*, *y*, and *z*) is determined, and then *a* is calculated.

3.2 Single Cylinder Research Engine Facility

The research engine facility (Figure 3-2) is based on a single cylinder Cooperative Fuel Research (CFR) engine, modified for Homogeneous Charge Compression Ignition (HCCI) operation and coupled to a dynamometer, and has been used extensively at Drexel University to study the autoignition and combustion of hydrocarbon fuel components and blends (Gong, 2005; Johnson, 2007). The key feature of this engine is a movable cylinder head that allows variation of the compression ratio from 4:1 to 18:1. For this study, the compression ratio was held at 16:1. The bore is 8.25 cm, the stroke is 11.43 cm, and the displacement is 611.6 cm^3. The intake valve opening (IVO), intake valve closing (IVC), exhaust valve opening (EVO), and exhaust valve closing (EVC) were 10° *b*TDC, 34° *a*BDC, 40° *b*BDC, and 15° *a*TDC, respectively, where TDC represents the piston at the top position, BDC is the piston at the bottom position, and *a* and *b* are after and before. Figure 3-3 shows a schematic of the engine at TDC, identifying key components and definitions. Engine geometry and operating conditions are listed in Table 3-1. To correlate the method of presenting in-cylinder pressure data as a function of crankshaft position with the physical process of a four-stroke engine, Figure 3-4 shows the crankshaft and other parts at key positions throughout the two-rotation cycle. Figure 3-4(a) shows a schematic of the engine at IVO. The intake stroke then occurs as fuel and air enter. Figure 3-4(b) shows a schematic at IVC, when the cylinder has unburned fuel and air. Next, the compression stroke occurs as the piston moves upward, followed by the power stroke, as the mixture ignites due to decreasing volume and subsequent increasing pressure. Figure 3-4(c) shows the engine at EVO, followed by the exhaust stroke as combustion products exit the cylinder. Figure 3-4(d) shows the

engine at EVC. As seen in Fig. 3-4 and as with most engines, there is a valve overlap period, such that before the exhaust valve closes, the intake valve opens for the following cycle.

The fuels were injected into the air stream of the heated inlet manifold well upstream of the intake valve to assure complete vaporization and mixing. The inlet temperature was set to 427 K, the inlet manifold pressure was 0.1 MPa, the equivalence ratio of the fuel-air mixture was 0.26, and the engine was operated at a speed of 750 RPM.

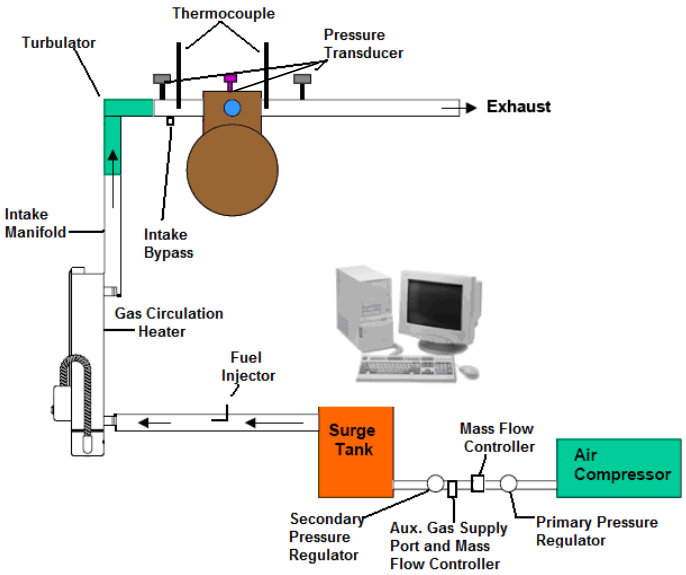

Figure 3-2: Schematic of the single cylinder research engine.

Table 3-1: Engine geometry and operating conditions.

Compression ratio	4:1 – 18:1	IVO	10° *b*TDC
Bore	8.25 m	IVC	34° *a*BDC
Stroke	11.43 cm	EVO	40° *b*BDC
Displacement	611.6 cm^3	EVC	15° *a*TDC
Inlet temperature	427 K	Equivalence ratio	0.26
Inlet pressure	0.1 MPa	Speed	750 RPM

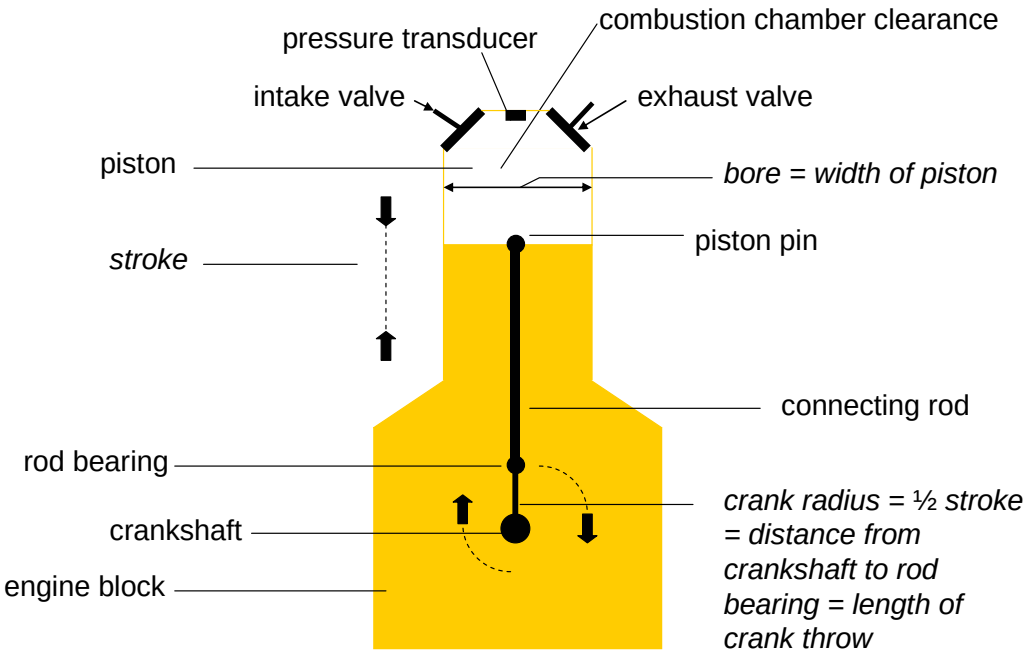

Figure 3-3: Engine schematic at TDC. Not drawn to scale.

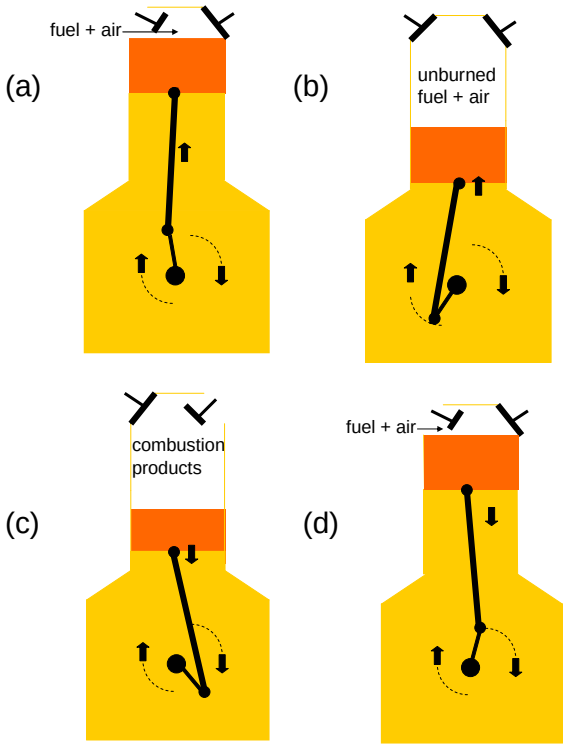

Figure 3-4: Engine piston position at (a) IVC (10° *b*TDC), (b) IVC (34° *a*BDC), (c) EVO 40° *b*BDC), and (d) EVC (15° *a*TDC).

In-cylinder pressure was measured with a piezoelectric pressure transducer at the port mounted in the cylinder head. Pressure was measured as a function of the crankshaft position, which was measured with a shaft encoder. Uncertainty in the crankshaft position is ±0.2 crank angle degrees (CAD). Each pressure trace shown is the average of 100 cycles with a coefficient of variation ≤ 5%. When characterizing the autoignition of fuels by their pressure traces, it is important to account for any pressure rise due to self-reactive heating. To examine the effect reactive self-heating of the mixture has on experimental autoignition timing, isentropic, non-reactive compression temperatures ($T_{\Delta S=0,\ Fuel/Air}$) were calculated.

Assuming Ideal Gas behavior, Eq. 3-3 expresses the non-reactive, isentropic in-cylinder temperature ($T_{\Delta S=0,\ Fuel/Air}$) for each crank angle after IVC.

$$T_{\Delta S=0,Fuel/Air} = \frac{\left(\frac{V_{@\,IVC}}{V}\right)^{\gamma} P_{@\,IVC} V}{nR} \tag{3-3}$$

Here $V_{@IVC}$ is the volume at IVC, $P_{@IVC}$ is the pressure at IVC (0.1 MPa), V is the instantaneous volume, n is the number of moles in the fuel/air mixture, and R is the universal gas constant. V is calculated as a function of crank angle using the engine geometry and standard piston motion equations (Ferguson and Kirkpatrick, 2001), Eq. 3-4

$$V = V_c + \left(\frac{-(cra)\cos(\frac{\pi CAD}{180^\circ}) - \sqrt{(cro)^2 - (cra)^2 \sin^2(\frac{\pi CAD}{180^\circ})} + cra + cro}{4} \right) \pi b^2 \tag{3-4}$$

Here *cra* is the crank radius (0.05715 m), *CAD* is the crank angle degree, *cro* is the connecting rod length (0.254 m), and *b* is the bore. The combustion chamber clearance volume V_c is from Eq. 3-5

$$V_c = \frac{\frac{\pi}{4} b^2 s}{CR - 1} \tag{3-5}$$

Here *s* is the stroke and *CR* is the compression ratio.

The specific heat ratio γ in Eq. 3-3 was calculated using the temperature-dependent specific heats. Polynomial equations for the gas-phase specific heat at constant pressure ($C_{p,g}$) for N_2 and O_2 are available from the literature (Chase, 1998). A natural logarithmic equation for $C_{p,g}$ of *n*-decane was formulated based on results reported in the temperature range of 273-1500 K (Scott, 1974). Natural logarithmic equations for $C_{p,g}$'s of *o*-xylene, *m*-xylene, and *p*-xylene were formulated from results reported in the temperature range of 273-1500 K for each of the isomers (Draeger, 1985). Natural logarithms and polynomials are common formats for relating the temperature-dependence of specific heat capacity at constant pressure.

Calculations for $T_{\Delta S=0,\ Fuel/Air}$ of the JP-8 samples used in this study were not conducted. Smith and Bruno (2007) worked on JP-8 characterization and identified and quantified 24 components at the 70% distillate fraction. Because these hydrocarbons included various linear and branched paraffins and alkylated cycloparaffins that do not have temperature-dependent specific heat values readily available, and because a significant proportion of the components are still lacking, any attempt at calculating $C_{p,g}$ would have led to a large uncertainty.

For comparison to experiments, the in-cylinder temperature rise, according to calculations for non-reactive, isentropic conditions, is shown in Figure 3-5. At the given engine speed, the time duration is 32.2 ms from IVC at 214 CAD to TDC. Thus, at TDC, $T_{\Delta S=0,\ Fuel/Air}$ = 1054 K. From IVC to TDC, the temperature range is 427-1054 K and the pressure range is 0.1-5 MPa for non-reactive, isentropic conditions. In the PFR, the low temperature regime begins around 600 K when the pressure is 0.8 MPa. However, because increasing pressure shifts the temperature regimes to higher temperatures, the low temperature regime in the engine may begin at $T_{\Delta S=0,\ Fuel/Air} > 600$ K. Specifically, 600 K is at 296 CAD in Fig. 3-5. The point of low temperature reactivity in the engine should occur at some CAD greater than 296, although the coupling of temperature and pressure, as well as equivalence ratio, makes an exact determination difficult.

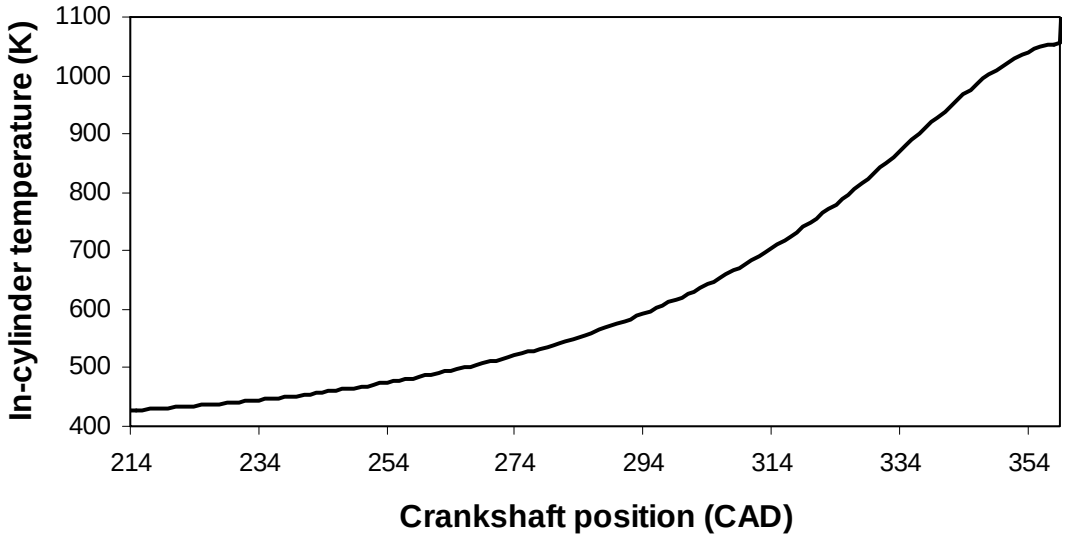

Figure 3-5: Temperature rise (calculated) due to isentropic compression of air at engine conditions, time = 0 ms at IVC and time = 32.2 ms at TDC.

3.3 Analytical Chemistry Facility

During the PFR experiments, samples were stored in a sample storage cart. The cart was originally designed by Koert (1990) and modified by Lenhert (2004a & b) and consists of an oven containing an electrically-actuated valve that controls the positioning for 16 10-mL stainless steel loops. Samples were stored in the cart at 453 K for chemical analysis after the completion of the PFR experiment.

Each sample from the storage cart was analyzed with a GC/MS/FID facility for species composition. Each sample was injected at 570 torr pressure. The GC used a Supelco Petrocol DH capillary column (100-m length, 0.5-μm film thickness, 0.25-mm OD, 1250 Phase Ratio (β)) for species separation; this column was designed for gasoline component separation. To aid in separation of lighter species, the GC column oven was temperature programmed from subambient temperatures, using liquid CO_2 cooling, to 250°C. Table 3-2 shows the temperature program for the GC.

Table 3-2: GC/MS operating parameters.

Gas Chromatograph		**Mass Spectrometer**	
Initial Temperature	-20 °C	Ion Source Temperature	200 °C
Initial Time	5 min	Scan Range	10-250 amu/z
Ramp 1 Rate	10 °C/min	Scan Rate	500 amu/sec
Ramp 1 Temperature	120 °C	Multiplier Voltage	1812 V
Ramp 1 Hold Time	0 min	Ionization Mode	Electron
Ramp 2 Rate	5 °C/min	Electron Energy	-70 eV
Ramp 2 Temperature	250 °C	Emission Current	100 μA
Ramp 2 Hold Time	5 min	Chromatographic Filter	4 sec
Post Analysis Temperature	275 °C		
Post Analysis Pressure	75 psi		
Post Analysis Time	10 min		

After separation, column flow was split between the MS and FID in a low dead volume split connection installed by Lenhert (2004a & b). Table 3-2 also shows operating parameters for the MS. Identification of species was conducted by comparing mass spectra from the MS to the NIST 2.0 MS database, which contains spectra for 150,000 compounds. Several methods of matching were used with the Thermo Electron XCalibur program. Search index (SI) compares the unknown spectrum to the library spectrum from the database. Reserve search index (RSI) compares the two spectra, but ignores any peaks in the unknown that are not in the library spectrum. Probability (Prob) determines a probability factor based on differences between similar library spectra. Additionally, GC retention time matching to calibration standards ensured species identification.

Quantification of species was attempted with the FID. Typically, FID area counts are used and compared to calibration runs to calculate quantities of intermediate species. However, the results were inconclusive with the fuels of this study. In some samples, *n*-dodecane quantities were erratic. For example, levels of *n*-dodecane showed no pattern, with quantities much greater in test samples with oxygen than in fuel calibration runs without oxygen. Also, *n*-dodecane was at significant levels during runs of calibration bottles of other species. Nevertheless, the goals of this study were still possible to achieve despite the quantification difficulties. After this series of experiments, the GC injection method was modified with a new heating system, as described by Kurman *et al*. (2009b), and this resolved the issue.

3.4 Gases and Fuels

All gases and fuels purchased for the experiments were of the highest purities possible. Table 3-3 lists all gases and fuels, manufacturers, and purity levels. Nitrogen and oxygen were used to create the synthetic air for the PFR experiments. The fuels were used for PFR and engine experiments, as well as for GC retention time matching and FID calibration efforts.

Table 3-3: List of experimental gases and fuels.

Component	Manufacturer	Purity, ≥
Nitrogen	Airgas	99.9%
Oxygen	Airgas	99.994%
n-dodecane	Sigma-Aldrich	99%
n-decane	Sigma-Aldrich	99%
p-xylene	Sigma-Aldrich	99%
o-xylene	Sigma-Aldrich	99%
m-xylene	Sigma-Aldrich	99%
methylcyclohexane	Sigma-Aldrich	99%
iso-octane	Sigma-Aldrich	99%
n-tetradecane	Sigma-Aldrich	99%
Tetralin	Sigma-Aldrich	99%
Toluene	Sigma-Aldrich	99.5%
o-tolualdehyde	AccuStandard	N/A*
m-tolualdehyde	AccuStandard	N/A*
p-tolualdehyde	AccuStandard	N/A*

* Component was part of a 15-component carbonyl mixture.

Samples of JP-8 were supplied by Wright-Patterson Air Force Base. Table 3-4 shows properties of the two JP-8 samples, provided by Edwards (2003), used in this study.

Table 3-4: Properties of the JP-8 samples.

Property	JP-8 POSF-4177	JP-8 POSF-3773
Aromatics (% Vol)	16.3	15.9
Olefin (% Vol)	0.9	0.7
Naphthalenes (% Vol)	1.0	N/A
American Petroleum Institute (API) gravity	42.4	45.8
Heat of Combustion (MJ/kg)	43.1	43.3
Hydrogen Content (% mass)	13.7	13.9
Fuel System Icing Inhibitor (FSII) (% Vol)	0.11	0.07
Total Sulfur (% mass)	0.14	0.07
Distillation (°C)		
Initial Boiling Point	129	150
10%	179	170
20%	187	176
50%	205	196
90%	235	237
Evaporation Point	261	256

Table 3-5 compares the composition of JP-8 POSF-3773, considered an "average" JP-8 sample, to a survey of JP-8, U.S. commercial jet fuel (Jet A), U.S. Navy jet fuel (JP-5), and Russian jet fuel (TS-1); this sample matches the average paraffin, naphthene, and aromatic content of jet fuel samples fairly well (Holley *et al.*, 2007). A more detailed chemical speciation has been conducted by Smith and Bruno (2007). o-Xylene was among the major components identified.

Table 3-5: Composition of "average" JP-8 and world survey average.

	JP-8 POSF-3773 (%)	World survey average of Jet A, JP-8, JP-5, and TS-1 (%)
Paraffins (*n*- and *i*-)	57.2	58.8
Cycloparaffins	17.4	10.9
Dicycloparaffins	6.1	9.3
Tricycloparaffins	0.6	1.1
Alkylbenzenes	13.5	13.4
Indans/Tetralins	3.4	4.9
Indenes	<0.2	<0.2
Naphthalene	<0.2	0.13
Naphthalenes	1.7	1.55
Acenaphthenes	<0.2	<0.2
Acenaphthylenes	<0.2	<0.2
Tricyclic Aromatics	<0.2	<0.2

CHAPTER 4. MODEL PARAMETERS

4.1 Chemkin Parameters

All modeling for this project was evaluated in Chemkin 4.1 (Kee *et al.*, 2006). The Plug Flow Reactor setup was used under isothermal conditions, with calculations for a reactor length of 40 cm at 0.5-cm intervals. For each simulation, the momentum equation was solved and the residence time was calculated. After performing several simulations to determine optimal tolerances, absolute and relative tolerance values were set to 1.0×10^{-14} and 1.0×10^{-12}, respectively.

Chemkin is commonly utilized in the combustion community. For the Plug Flow Reactor setup, the software solves the equations for mass continuity, gas-species conservation, energy, momentum, and surface site species conservation. The setup assumes no mixing in the axial direction and complete mixing in the transverse direction to that. The system is modeled using first-order ordinary differential equations. No transport properties are needed for the Plug Flow Reactor setup. Thermodynamics properties are needed for the specific enthalpy, heat capacity, and entropy of the species. These parameters can be supplied as standard NASA polynomials into Chemkin (Reaction Design, 2007a). For the solution of the chemistry, the pre-exponential factor, temperature exponent, and activation energy are required for each Arrhenius equation.

To determine the dominant low temperature reaction pathways of xylene, a rate-of-production (ROP) analysis was conducted. The analysis is a feature of Chemkin 4.1 and identified how each reaction involving a selected species, either as a reactant or

product, contributes to the net molar fraction of the species. From Reaction Design (2007b), Eq. 4-1 gives P_k, the molar production of a species per unit volume

$$P_k = \dot{\varpi}_k + \sum_{m=1}^{M} \frac{A_m}{V} \dot{s}_{k,m} = \sum_{i=1}^{I} \nu_{ki} q_i + \sum_{m=1}^{M} \frac{A_m}{V} \sum_{i=1}^{I_s} \nu_{ki}^s q_i^s \qquad \text{(Eq. 4-1)}$$

In Eq. 4-1, ν_{ki} and ν^s_{ki} are the stoichiometric coefficients for the gas and surface reactions, respectively, and q_i and q^s_i are the rate of progress of the I gas-phase reactions and the I_s surface reactions. The surface area of the material m is A_m where reaction i is involved. For this work, no surface reactions are modeled or assumed to occur experimentally. The contribution to the rate of production of species k from gas-phase reaction i is from Eq. 4-2

$$C_{ki} = \nu_{ki} q_i \qquad \text{(Eq. 4-2)}$$

Thus, ROP analysis is a powerful means of identifying key reactions, and when done with multiple species, identifying key reaction pathways. The data at 700 K was used, where reactivity is high and several different pathways would potentially be activated. The ROP for each reaction producing a major aromatic species at 120 ms residence time (40 cm along the reaction tube) were collected. The reaction with the maximum absolute value ROP was identified. All reactions that contributed a value of at least 5% of the maximum ROP (either forward or reverse) were considered significant for analysis.

4.2 Politecnico di Milano Model

The majority of the modeling performed for this project utilized the large hydrocarbon chemical kinetic model of Ranzi *et al.* (2007). The model, an ongoing project at Politecnico di Milano, is described by Ranzi *et al.* (2005), and will be called the

Ranzi model. The model contains 310 species and 8,011 reactions, and has an associated thermochemistry file. The model is a semi-detailed mechanism describing the pyrolysis, partial oxidation, and combustion of hydrocarbon fuels up to C_{16} and is applicable for low and high temperatures. *n*-Dodecane oxidation is included in the model, but it must be noted that the xylene submechanism lumps the three isomers as one xylene species. The uniqueness of the Ranzi model is that it includes *n*-dodecane and xylene together, so that mixtures can be studied. Additionally, unlike other models available at the start of this study, the model includes the low temperature chemistry for *n*-dodecane. This low temperature submechanism was based primarily on the experimental work of Agosta *et al.* (2004) studying *n*-dodecane in the Drexel PFR facility. While the model has not been widely validated, it is the best possible model for these conditions.

4.3 CNRS Model

A *m*-xylene chemical kinetic model (189 species, 1,359 reactions) was supplied by Gaïl and Dagaut (2007) at CNRS in France with a file of the thermochemistry. The model is a detailed mechanism for the combustion of *m*-xylene and its development was based primarily on the experimental behavior of *m*-xylene oxidized in a jet-stirred reactor at high temperatures (900-1400 K). However, the CNRS modeling group did not have a low temperature *n*-dodecane model. Because modeling was not a primary objective of this study, no attempt was made to model *n*-dodecane / xylene mixtures utilizing the CNRS xylene model and a *n*-dodecane model, but this is possible for future work.

CHAPTER 5. PREIGNITION RESULTS

5.1 Preliminary Work

Because xylene had never been tested in the PFR prior to this study, a preliminary experiment was conducted to establish the best conditions of temperature, pressure, equivalence ratio, and dilution to study low temperature reactivity in a safe laboratory environment. A mixture of 85% *n*-decane / 15% *m*-xylene by liquid volume was oxidized at 8.0 atm pressure, 0.30 equivalence ratio, 0.120 s residence time, and 600-800 K temperatures. Figure 5-1 shows CO and CO_2 production from the experiment. The NTC behavior characteristic of *n*-alkanes was observed and expected, as the mixture was largely composed of *n*-decane. No experimental issues with using xylene were identified.

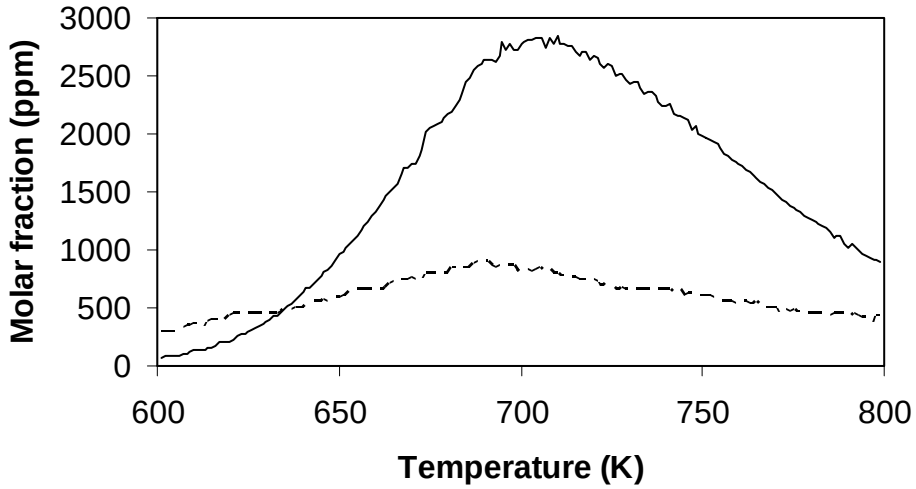

Figure 5-1: CO (—) and CO_2 (---) production from 85% *n*-decane / 15% *m*-xylene oxidized in the PFR.

5.2 Neat Xylenes in the PFR

To investigate the preignition behavior of neat xylenes in the PFR, neat *o*- and *m*-xylene were each tested at 0.30 equivalence ratio, 0.120 s residence time, 8 atm pressure, and 600-832 K temperatures. The composition of the test mixture was, in molar fractions, 0.00120 (1200 ppm) xylene (o- and m- separately), 0.957 N_2, and 0.0420 O_2. CO and CO_2 were monitored, but none was produced, indicating that the neat fuel was not reactive. Furthermore, an electrochemical oxygen measuring cell was acquired and installed during the course of the project for online measuring of O_2. Additional experiments were conducted and no significant reduction in O_2 was observed, further confirming the non-reactive nature of the neat xylenes under the test conditions. As the *o*-xylene and *m*-xylene experiments were conclusive, and *p*-xylene exhibits similar reactivity, no *p*-xylene experiment was conducted.

5.3 Xylene / *n*-Dodecane Mixtures in the PFR

Mixtures of xylene with *n*-dodecane were oxidized in the PFR to evaluate the reactivity of xylene when a second, reactive component is added. Table 5-1 lists the three experiments and conditions. Compositions of 77% *n*-dodecane / 23% xylene by volume were selected because the Jet Fuel Surrogate Working Group (2008) recommended a JP-8 surrogate composed of 77% *n*-dodecane / 23% *m*-xylene for modeling soot formation. All experiments were conducted at 0.8 MPa pressure. Several fuel concentrations, equivalence ratios, and temperature ranges were tested during the experimental program and specific values are noted for each experiment.

Table 5-1: Experimental conditions for PFR experiments for liquid fuel composition of 77% *n*-dodecane / 23% xylene

Xylene molar fraction (ppm)	Equivalence ratio	*n*-Dodecane molar fraction (ppm)	Oxygen molar fraction (ppm)	Nitrogen molar fraction (ppm)	Temperature range (K)	Pressure (MPa)	Residence time (ms)
165 *o*-	0.23	295	31,500	968,040	600-837	0.8	110
165 *m*-	0.23	295	31,500	968,040	600-834	0.8	110
284 *p*-	0.30	516	42,000	960,000	600-811	0.8	120

Figure 5-2 shows the reactivity map of the PFR experiment with 77% *n*-dodecane / 23% *o*-xylene. The experiment was conducted at an equivalence ratio of 0.23, residence time of 0.110 s, and a temperature range of 600-837 K. The diluted mixture was composed of, in molar fractions, 0.00046 (460 ppm) fuel (molecular formula of $C_{10.6}H_{20.3}$), 0.96804 N_2, and 0.03150 O_2. The fuel consisted of 295 ppm *n*-dodecane and 165 ppm *o*-xylene. The mixture exhibited the characteristic NTC behavior common among reactive hydrocarbons at these temperatures and pressure. Specifically for this mixture, significant reactivity (>150 ppm CO) was observed at 628 K, and increased with increasing temperature until peak reactivity, 1030 ppm CO, occurred at 699 K. Reactivity then decreased with increasing temperature in the NTC region. Significant reactivity was observed until 797 K, and by the maximum temperature of 837 K, no CO was produced. CO_2 showed similar trends at approximately 1/3 the production level.

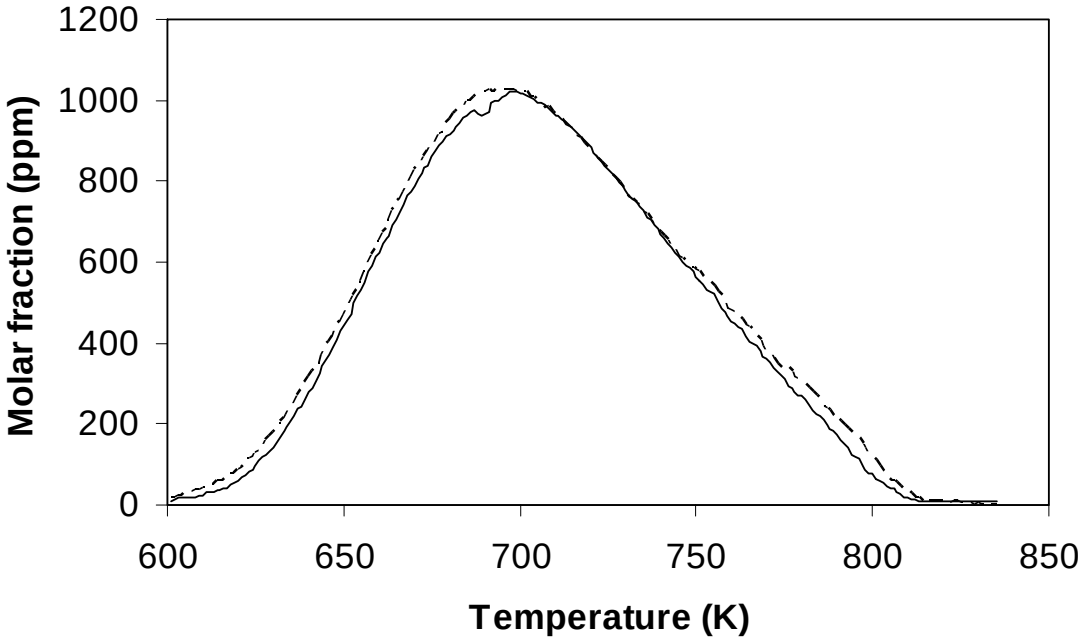

Figure 5-2: CO from (- - -): *o*-xylene mixture, (—): *m*-xylene mixture.

Stable intermediate species were collected at 15 temperatures during the *n*-dodecane / *o*-xylene experiment in the PFR and analyzed with GC/MS/FID. At 837 K, a sample was collected before O_2 was introduced into the PFR, for fuel calibration purposes and to check for fuel cracking. Only the parent fuels were identified in this sample. After O_2 was introduced, over 30 intermediate species were identified in the remaining samples. Most of them can largely be attributed to *n*-dodecane oxidation, including linear alkenes (ethene, propene, 1-butene, 1-pentene, 1-hexene, 1-octene, 1-nonene, 1-decene, and several dodecene isomers), saturated aldehydes (acetaldehyde, propanal, butanal, pentanal, hexanal, and heptanal), unsaturated aldehydes (2-propenal, 2-methyl-2-propenal, and 2-methyl-2-butenal), enones (methyl vinyl ketone), and ketones (2-butanone, 2-pentanone, and 2-hexanone). These results agree with a previous investigation of *n*-dodecane oxidation in the PFR (Lenhert, 2004a). Several cyclic ethers

(2-methyl-tetrahydrofuran and 2-butyl-tetrahydrofuran) and an alkylated furan (2-methylfuran) were identified in this experiment but not in the previous neat *n*-dodecane experiment. However, the GC/MS/FID technique had been improved since the previous study to reduce noise so that species with lower concentrations could now be identified, and it was suspected that these were produced from the *n*-dodecane. Later neat n-dodecane work confirmed this (Kurman *et al.*, 2009a). Nonetheless, aromatic species were identified (*o*-tolualdehyde and toluene) and attributed to *o*-xylene oxidation. Table 5-2 shows the key species relevant for this study, including the parent fuels, and the temperatures where they were identified. As mentioned, a sample was also taken at 837 K before O_2 introduction, and only *o*-xylene and *n*-dodecane were identified in that sample.

Table 5-2: Key species identified from the 77% *n*-dodecane / 23% *o*-xylene PFR experiment, temperatures in K.

Species	625	650	670	680	690	705	720	740	760	775	800	805	815	825
o-Tolualdehyde	X	X	X	X	X	X	X	X	X	X	X	X	X	X
Toluene	X	X	X	X	X	X	X	X	X	X	X	X	X	
o-Xylene	X	X	X	X	X	X	X	X	X	X	X	X	X	X
n-Dodecane	X	X	X	X	X	X	X	X	X	X	X	X	X	X

Figure 5-2 also shows the results of the PFR experiment with 77% *n*-dodecane / 23% *m*-xylene, oxidized under the same conditions as the aforementioned experiment with *o*-xylene. The results are similar, with a maximum of 1030 ppm CO produced at 693 K. Figure 5-2 clearly indicates that there is no difference in CO production between *m*-xylene and *o*-xylene in the low temperature regime.

The same GC/MS/FID method was followed for the *n*-dodecane / *m*-xylene experiment as for the *n*-dodecane / *o*-xylene experiment. Similar results were found,

except that *m*-tolualdehyde was identified instead of *o*-tolualdehyde. Table 5-3 shows the corresponding key species. Again, a sample collected at 834 K before O_2 was introduced showed no fuel pyrolysis. Only *m*-xylene and *n*-dodecane peaks were observed in that sample.

Table 5-3: Key species identified from the 77% *n*-dodecane / 23% *m*-xylene PFR experiment, temperatures in K.

Species	625	650	670	680	690	705	720	740	760	775	800	805	815	825
m-Tolualdehyde	X	X	X	X	X	X	X	X	X	X	X	X	X	X
Toluene	X	X	X	X	X	X	X	X	X	X	X	X	X	
m-Xylene	X	X	X	X	X	X	X	X	X	X	X	X	X	X
n-Dodecane	X	X	X	X	X	X	X	X	X	X	X	X	X	X

A mixture of 77% *n*-dodecane / 23% *p*-xylene was also tested in the PFR with GC/MS/FID analysis. Because of low GC peaks in the previous experiments due to low fuel concentrations, the *n*-dodecane / *p*-xylene experiment was run at a higher fuel concentration (800 ppm fuel), equivalence ratio (0.30), and residence time (0.120 s). The O_2, N_2, and fuel molar fractions were 0.96, 0.042, and 0.0008, respectively. The fuel was composed of 516 ppm *n*-dodecane and 284 ppm *p*-xylene. Figure 5-3 shows the reactivity map of the PFR experiment. Significant reactivity was observed by 602 K, and continued through 811 K when the experiment was stopped. A maximum of 2450 ppm CO was produced at 700 K before the NTC region started. The same GC/MS/FID method was followed as for the previous mixtures. Aromatic species identified were *p*-tolualdehyde, toluene, and *p*-cresol. Of note, *p*-cresol was identified in this experiment but its *ortho*- and *meta*- isomers were not identified in the *o*-xylene and *m*-xylene

experiments. This may be because of the higher fuel concentration in the *p*-xylene experiment.

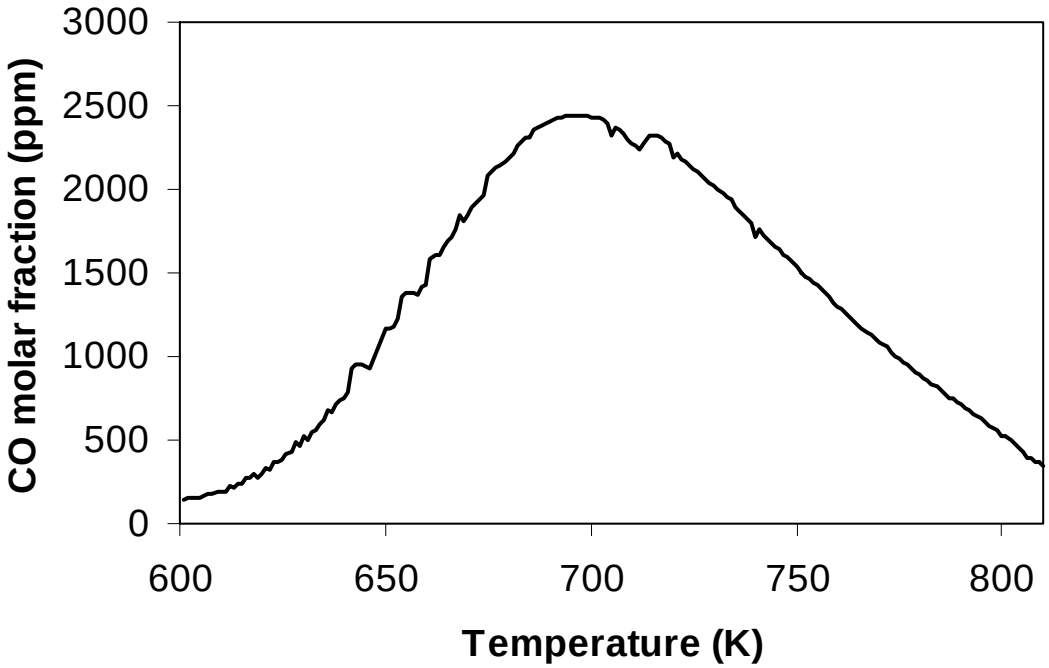

Figure 5-3: CO from *n*-dodecane / *p*-xylene mixture.

Quantification of intermediates was also planned for the *n*-dodecane / xylene mixture PFR experiments. However, the FID results were erratic and indicated experimental sampling issues. For example, FID area counts for *n*-dodecane were higher in samples where oxygen was added and at temperatures where reactivity was observed with the NDIR analyzer than in the calibration sample without oxygen. If sampling was maintaining the sample properly until analysis, the *n*-dodecane area counts for those samples with much reactivity should have been significantly lower than the calibration sample. The area count results suggested non-uniform condensation and subsequent

re-vaporization of *n*-dodecane somewhere from the PFR to the GC, such as in the heated, insulated transfer lines from the PFR to the storage cart, in the loops and valves in the cart, in the heated, insulated transfer line from the cart to the GC, or in the injection valve to the GC. As there were several possibilities in identifying the condensation and re-vaporization of *n*-dodecane on the level of hundreds of ppm, this was a lengthy process. PFR experiments for this study were finalized before the source of the problem was identified. However, the objectives of this project could be satisfied without intermediate species quantification experiments. Subsequently, new insulation and heating were later added to the 1-mL stainless steel sample loop, where the sample is stored before GC injection. This solved the problem of erratic *n*-dodecane FID area counts. As quantification involves measuring species in terms of concentration in a mixture, the erratic *n*-dodecane levels eliminated the possibility of quantifying intermediates.

5.4 Neat *n*-Dodecane in the PFR

To provide a baseline for the reactivity of the mixtures, experiments were conducted for neat *n*-dodecane in the PFR under the same conditions (pressure, equivalence ratio, nitrogen dilution, and residence time) as the n-dodecane / (*o*- and *m*-) xylene mixtures. Figure 5-4 compares the CO production of this experiment, with the 77% *n*-dodecane / 23% *m*-xylene experiment and the simulations of a CO profile from *n*-dodecane if the *m*-xylene was not reactive (64% of the CO by mole produced by the neat *n*-dodecane experiment, since the mixture contains 64% *n*-dodecane by molar fraction). Neat *n*-dodecane produced a maximum of 1540 ppm CO at 697 K. The projection of

77% *n*-dodecane / 23% non-reactive species produced 990 ppm CO, 40 ppm CO less than the actual results of 77% *n*-dodecane / 23% *m*-xylene. It appears that the xylene had a minimal effect on the expected overall reactivity of the mixtures for preignition conditions.

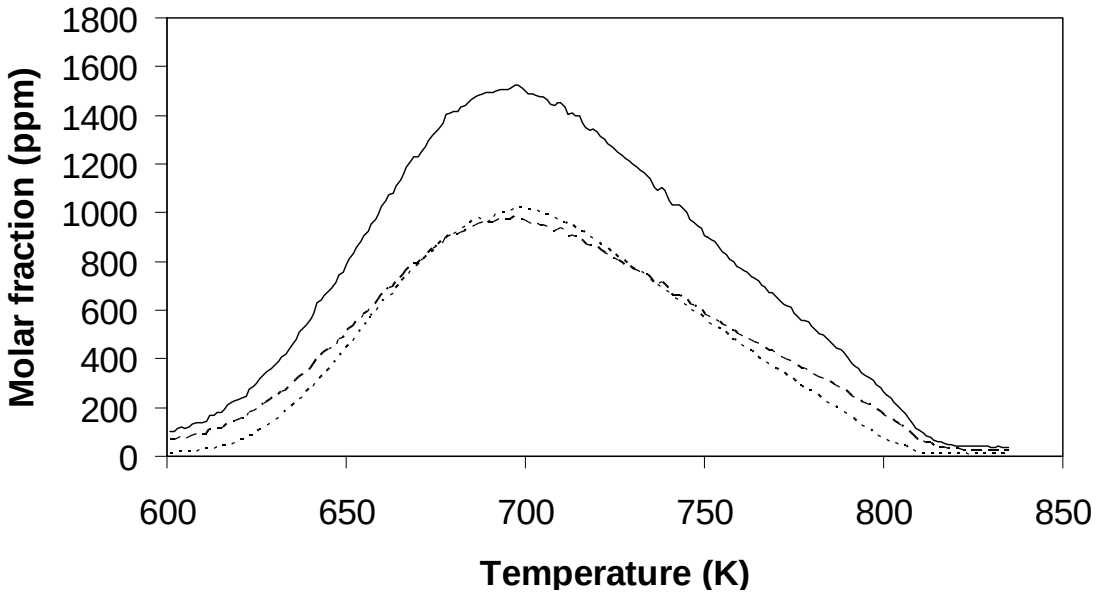

Figure 5-4: CO from (—): *n*-dodecane, (····): 77% *n*-dodecane / 23% *m*-xylene, (- - -): calculation for 77% *n*-dodecane / 23% non-reactive species.

5.5 JP-8 in the PFR

Since the mixture of 77% *n*-dodecane / 23% *m*-xylene was selected based on a recommendation for matching JP-8 soot formation, a sample of JP-8 (POSF-3773), previously determined to be of "average" reactivity and composition (Natelson *et al.*, 2008), was tested under the same conditions. Figure 5-5 shows a comparison between the mixture and JP-8. Both experiments were run at 0.23 equivalence ratio, 0.110 s residence time, and 8 atm pressure. As the actual empirical formula for JP-8 was

unknown, an average formula of $C_{11}H_{21}$ (H/C = 1.91) recommended by Edwards and Maurice (2001) was used to determine the liquid fuel flow rate, 1.050 mL/min, for maintaining the same equivalence ratio and nitrogen dilution as for the mixture. The JP-8 produced a maximum of 540 ppm CO at 694 K. Thus, the mixture was approximately twice as reactive as the JP-8 under preignition conditions, and would be a poor choice for a surrogate for these conditions. Nevertheless, the surrogate may still be a good choice for its initial selection of matching JP-8 soot formation, as the sooting phenomenon is a high temperature process. These observations and results highlight the difficulty in developing a single surrogate for all performance criteria.

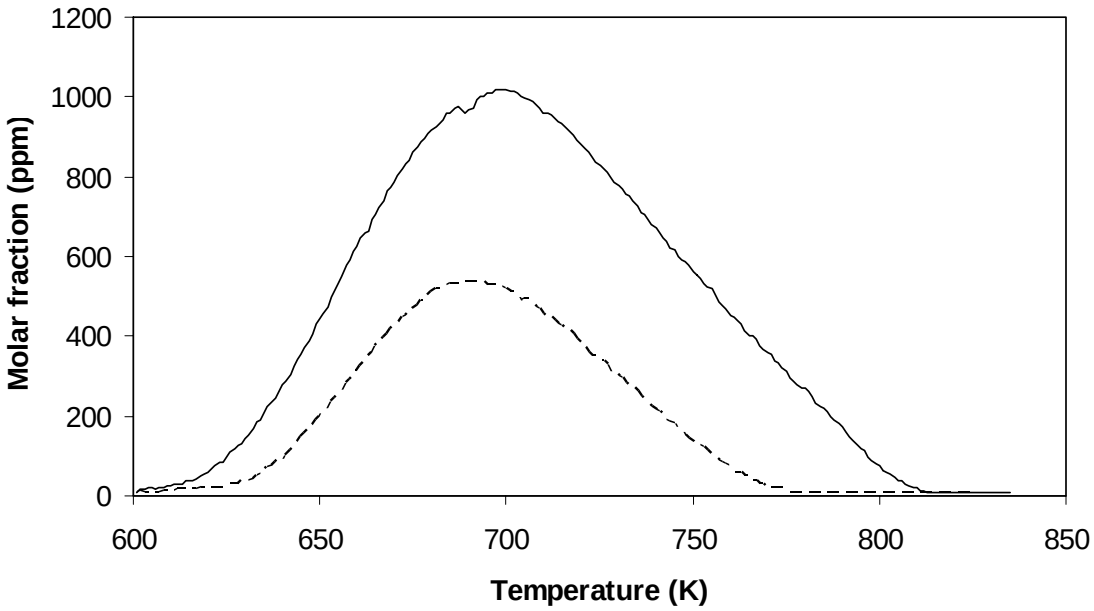

Figure 5-5: (—): CO from 77% *n*-dodecane / 23% *m*-xylene; (- - -): CO from JP-8-3773, considered to be a sample of "average" reactivity and composition.

5.6 Summary

A series of experiments was conducted in the PFR to study the low temperature oxidation of the xylene isomers. The significant findings, applicable for lean stoichiometry and in the low temperature regime, are:

(1) The xylene isomers, neat, show no reactivity,

(2) In binary mixtures with a more reactive component, each of the xylenes is reactive, but their reactivity is comparable, providing confirmation that the isomers may be lumped together in chemical kinetic modeling such that,

   (a) Each isomer produces its respective tolualdehyde isomer and toluene, and

   (b) The xylene does not affect the overall reactivity of the mixture, and

(3) A mixture of 77% n-dodecane / 23% m-xylene by volume is significantly more reactive than “average” JP-8.

CHAPTER 6. AUTOIGNITION RESULTS

6.1 Neat Xylenes in the Engine

To explore the relative reactivity of the xylene isomers under autoignition conditions, experiments were also conducted in the single cylinder CFR engine. *p*-Xylene, *m*-xylene, and *o*-xylene were each run neat and the in-cylinder pressure traces recorded. The pressure traces were identical to a motored run, indicating no energy release or reactivity under the given conditions outlined in Section 3.2 (0.26 equivalence ratio, 750 RPM engine speed, 427 K inlet temperature, 1 bar inlet pressure). Figure 6-1 shows the pressure traces of the four tests. Any potential effects of the variation in heat capacity and thermochemistry of the reactant mixture, due to the addition of large hydrocarbons, were minimal because of the very lean equivalence ratio.

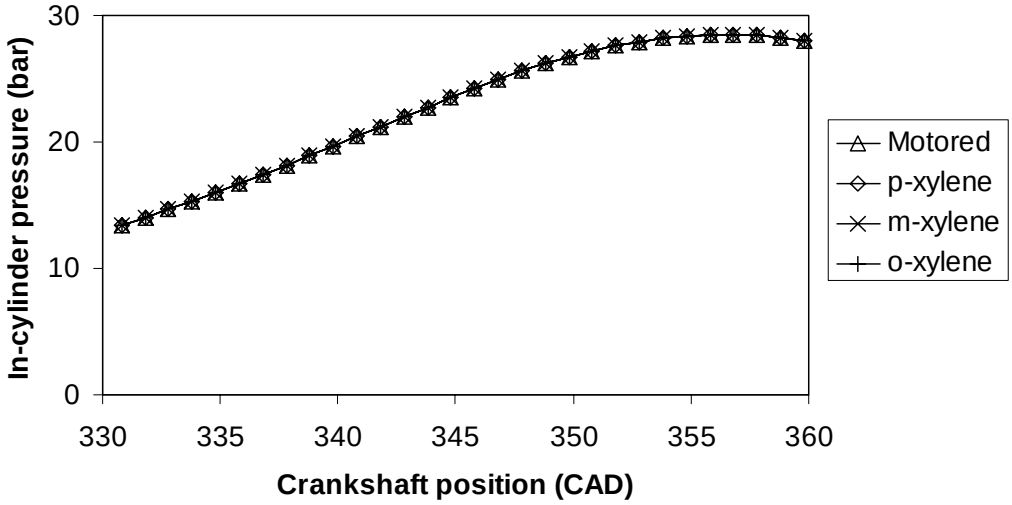

Figure 6-1: Pressure traces of neat xylenes and a motored run.

6.2 Xylene / *n*-Decane Binary Mixtures in the Engine

Because the neat xylenes were not reactive in the engine under the given conditions, *n*-decane was added to increase the radical pool and potentially initiate reactivity of the xylene. Since these experiments were conducted before the Jet Fuel Surrogate Working Group recommended the 77% *n*-dodecane / 23% *m*-xylene surrogate (2008), these xylene / paraffin binary mixtures were different from those used in the PFR. In the engine, mixtures of 85% *n*-decane / 15% xylene were studied, with fractions selected because the Violi *et al.* (2002) surrogate contains 15% xylene. Figure 6-2 shows data from the autoignition regime of the engine cycle, with emphasis on the portion relevant to autoignition. The x-axis refers to the position of the crankshaft, with 360 CAD (crank angle degrees) being TDC compression. A motored run with no fuel is shown to display the in-cylinder pressure rise due to compression of air. The binary mixtures with *p*-xylene or *m*-xylene showed combustion onset at 334.0 CAD. The mixture with *o*-xylene reacted slightly sooner, at 333.0 CAD, but within the CAD uncertainty of ±0.2 CAD.

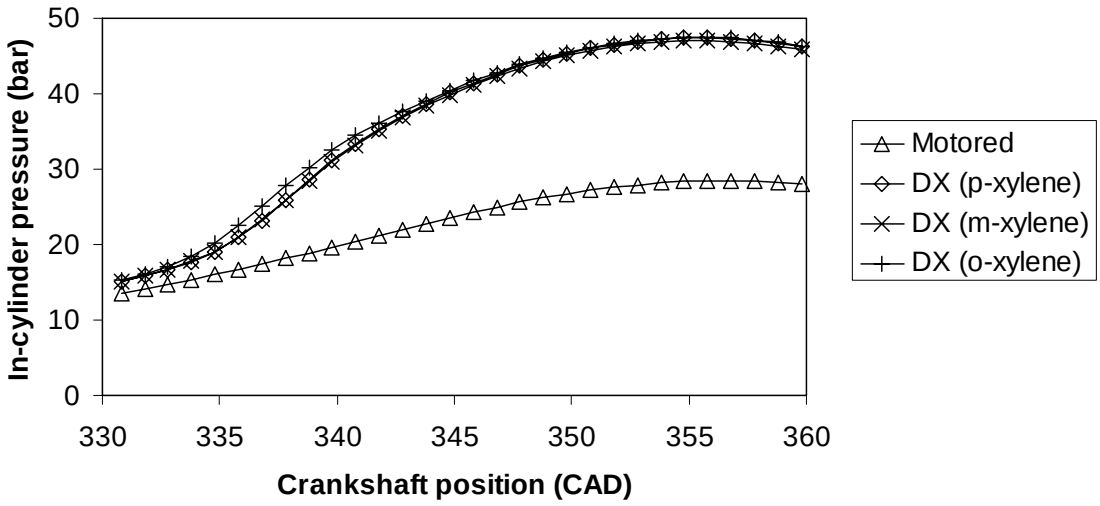

Figure 6-2: Autoignition of DX = 85% *n*-decane / 15% xylene by liquid volume.

To check that the autoignition differences are due to chemical reactions and not non-reactive heating, in-cylinder temperatures for non-reactive, isentropic conditions were calculated. The results for the different xylene isomers are within 1 K, due to the small differences in specific heat and the small fraction of xylene in the fuel-air mixture. Figure 6-3 shows the calculations for $T_{\Delta S=0,\ Fuel/Air}$ for the *n*-decane / *o*-xylene mixture, as a representative for all the binary mixtures. The temperature at TDC was 1002 K. At 333 CAD, where the *n*-decane / *o*-xylene mixture auto ignited, $T_{\Delta S=0,\ Fuel/Air}$ = 828 K. For the *n*-decane / *m*-xylene and *n*-decane / *p*-xylene mixtures, $T_{\Delta S=0,\ Fuel/Air}$ = 828 K, also, at 333 CAD. Therefore, the differences in autoignition timing are due to chemical reactions varying among the xylene isomers, and not heating of the fuels.

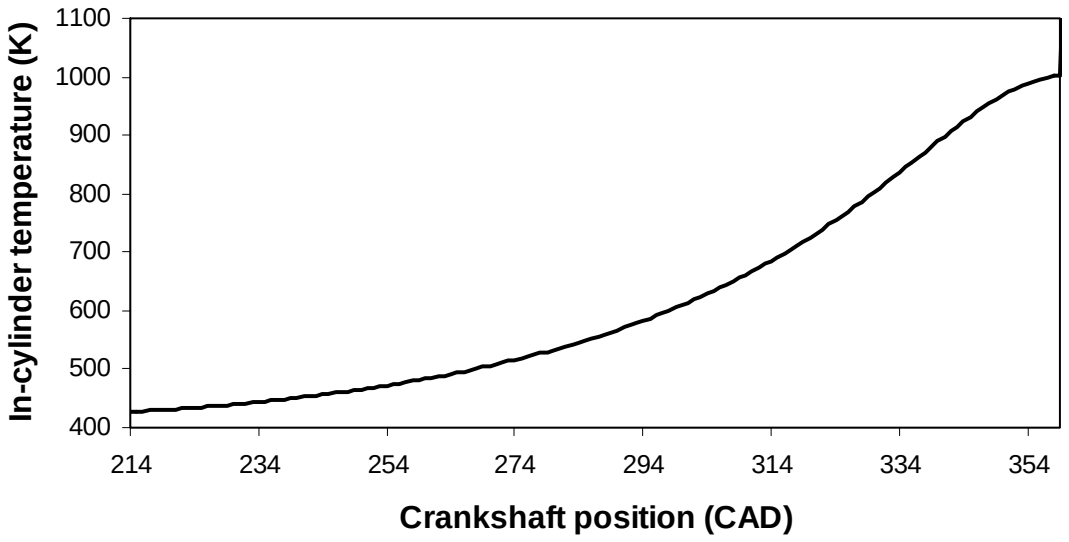

Figure 6-3: Temperature rise (calculated) due to non-reactive, isentropic compression of nitrogen / oxygen / *n*-decane / *o*-xylene mixture at engine conditions, time = 0 ms at IVC and time = 32.2 ms at TDC. Data with all three xylene isomers were identical.

6.3 JP-8 in the Engine

Two samples of JP-8 were tested under the given conditions for comparison. A broader series of JP-8 experiments was undertaken in the engine under different conditions (Johnson *et al.*, 2005). In the current study, JP-8 POSF-4177 showed onset of combustion at 343 CAD. JP-8 POSF-3773, considered "average" JP-8, showed onset of combustion slightly sooner, at 342 CAD. Results, shown in Figure 6-4, are discussed further in Sec. 6.4 as they relate to the JP-8 surrogate mixtures.

6.4 JP-8 Surrogates in the Engine

The Violi *et al.* (2002) surrogate was tested with each of the xylene isomers. Figure 6-4 shows the pressure traces, compared to the two samples of JP-8. The surrogate with either *m*-xylene or *p*-xylene showed onset of combustion at 341 CAD.

However, the surrogate with *o*-xylene showed slightly different behavior, with combustion onset sooner at 339 CAD. The original Violi surrogate with *m*-xylene matched JP-8 better than the modified Seshadri surrogate with *o*-xylene.

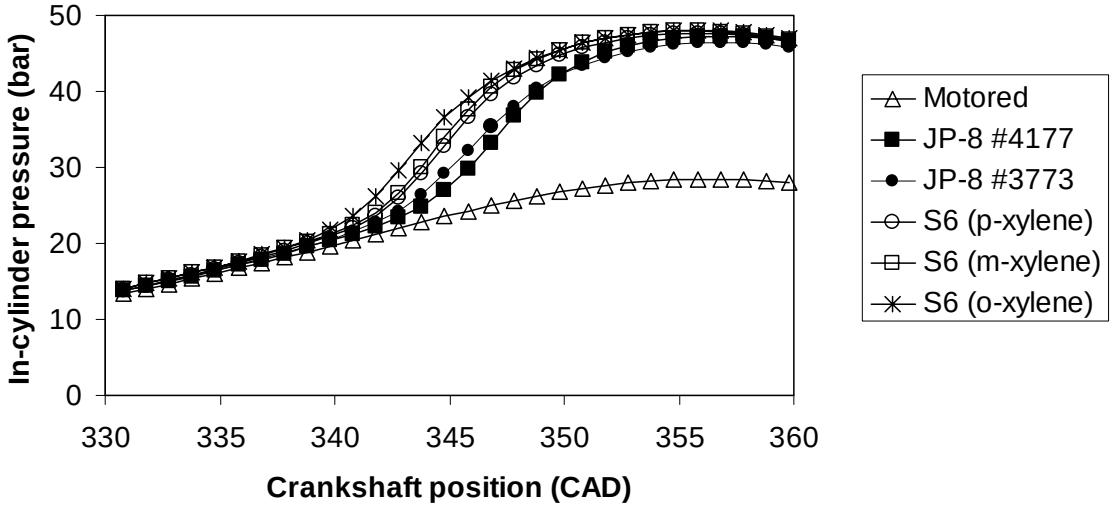

Figure 6-4: Autoignition of S6 = 15% xylene / 10% *iso*-octane / 20% methylcyclohexane / 30% *n*-dodecane / 20% *n*-tetradecane / 5% tetralin by liquid volume; JP-8-3773 has "average" reactivity and composition of JP-8.

6.5 Summary

A series of experiments was conducted in the research engine to study the autoignition of the xylene isomers. The significant findings, applicable for lean stoichiometry and at autoignition, are:

(1) The xylene isomers, neat, show no reactivity,

(2) In binary mixtures with a more reactive component, the xylenes are reactive, but *o*-xylene is slightly more reactive than *m*- or *p*-xylene,

(3) The Violi *et al.* (2002) JP-8 surrogate with *m*-xylene, as originally suggested, matches "average" JP-8 better in the research engine than the surrogate with *o*-xylene as tested by Seshadri (2006).

CHAPTER 7. MODELING ANALYSIS

7.1 Politecnico di Milano Model

The semi-detailed low-to-high temperature large hydrocarbon oxidation model of Ranzi *et al.* (2007) was evaluated under the PFR experimental conditions. Simulating the neat xylene experiments in the PFR, the model predicted no reactivity, corresponding with the experimental results. To better understand and analyze the xylene model, further simulations of mixtures, similar to the PFR experiments, were evaluated.

A mixture composed of molar fractions of 0.96804 N_2, 0.0315 O_2, 0.00029456 n-dodecane, and 0.00016544 xylene was evaluated to simulate the *n*-dodecane / xylene PFR experiments. Figure 7-1 shows the concentration of xylene and key stable intermediates, phenol and cyclopentadiene, attributed to xylene decomposition over the reaction temperatures. A maximum of 65% of the xylene was consumed, at 660 K. Figure 7-2 shows the model predictions of CO and CO_2 production with comparison to the experiments. The model captured the general trend of NTC behavior, although the peak CO formation was under predicted, at a significantly lower temperature (665 K) and level (600 ppm). Furthermore, the model predicted continuing reactivity to higher temperatures when the experimental reactivity ceased by 815 K. This behavior was not observed in the experiments. Nevertheless, the predictions captured the general behavior quite well, considering that the existing model was not developed with any special consideration for xylene preignition chemistry and was unmodified for this work.

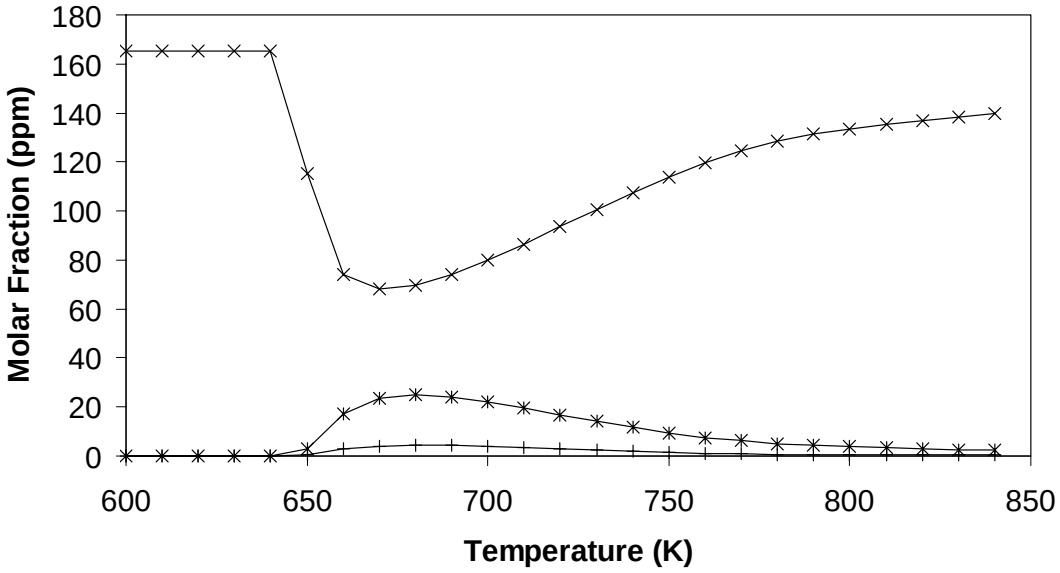

Figure 7-1: Species quantification from modeling 77% *n*-dodecane / 23% xylene oxidation: (x): xylene, (*): phenol, (+): cyclopentadiene.

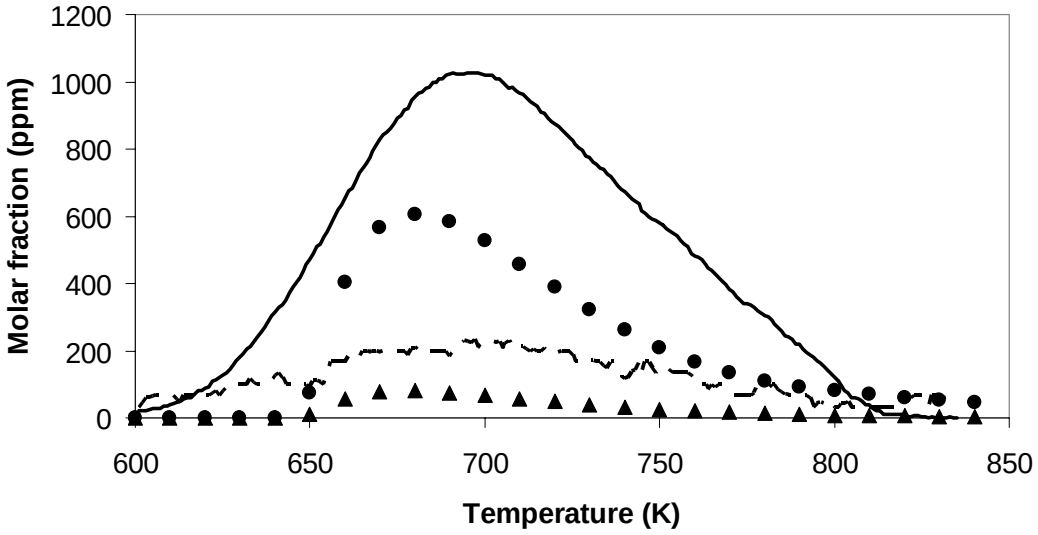

Figure 7-2: Oxidation of 77% *n*-dodecane / 23% xylene in the PFR: (—): CO experimental, (●): CO modeling, (--): CO_2 experimental, (▲): CO_2 modeling.

To determine the dominant low temperature reaction pathways of xylene, a rate-of-production-and-destruction analysis was conducted. The data at 700 K were used,

where reactivity is high and several different pathways would potentially be active. The ROP's (rate-of-production) for each reaction producing a major aromatic species at 120 ms residence time (40 cm along the reaction tube) were collected. The ROP was done at 120 ms because that is when the mixture reactions are quenched and samples analyzed to obtain speciation information. In the experiments, all species were measured after the mixture reacted for 120 ms and therefore model results can only be accurately compared to this experimental residence time. While determining ROP values at lesser residence times is feasible, the selection of 120 ms residence time for ROP analysis is to directly identify the reactions responsible for the products measured experimentally. All reactions that contributed a value of at least 5% of the maximum ROP (either forward or reverse) were considered significant for analysis.

The model includes 102 reactions involving xylene, many of them reversible. The ROP for xylene was -3.02×10^{-9} mol*cm^{-3}*s^{-1}. The dominant pathway for xylene destruction was via R1 (#4417 as Chemkin 4.1 formats the model), producing the xylyl radical (C_8H_9). Another significant pathway was via R2 (#4458), producing the methylphenyl radical (C_7H_7), water, and ethene. R2 is an example of a global reaction, meant to reduce the number of reactions in the model. Xylene was also produced from the reverse of R3 (#729). Figure 7-3 compares the ROP of these major reactions.

$$OH + C_8H_{10} \Rightarrow H_2O + C_8H_9 \qquad \text{R1 (4417)}$$

$$OH + C_8H_{10} \Rightarrow H_2O + C_7H_7 + 0.5 * C_2H_4 \qquad \text{R2 (4458)}$$

$$O_2 + C_8H_{10} \Leftrightarrow HO_2 + C_8H_9 \qquad \text{R3 (729)}$$

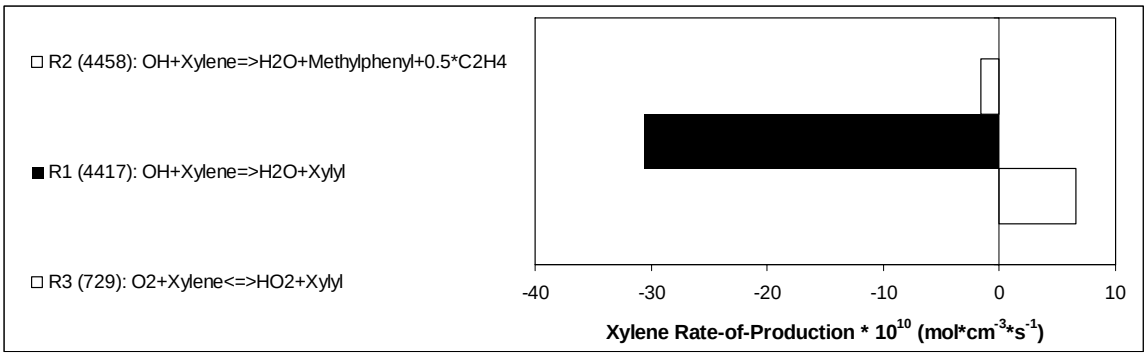

Figure 7-3: Key reactions involving xylene destruction and production.

The ROP for the xylyl radical was -2.03×10^{-11} mol*cm^{-3}*s^{-1}. Of 82 reactions involving xylyl radical, Figure 7-4 shows the significant reactions. R1, production of xylyl radical from xylene, was the dominant pathway. The main pathway for destruction was R4 (#794), leading to a phenyl radical (C_6H_5) and smaller species. Another significant pathway for xylyl radical destruction was the reversible path of R3, as mentioned for xylene production. An additional reaction for xylyl radical destruction was in the production of benzaldehyde, R5 (#793).

$$HO_2 + C_8H_9 \Rightarrow C_6H_5 + CH_2O + OH + 0.5 * C_2H_4 \qquad \text{R4 (794)}$$

$$HO_2 + C_8H_9 \Rightarrow C_7H_6O + H + OH + 0.5 * C_2H_4 \qquad \text{R5 (793)}$$

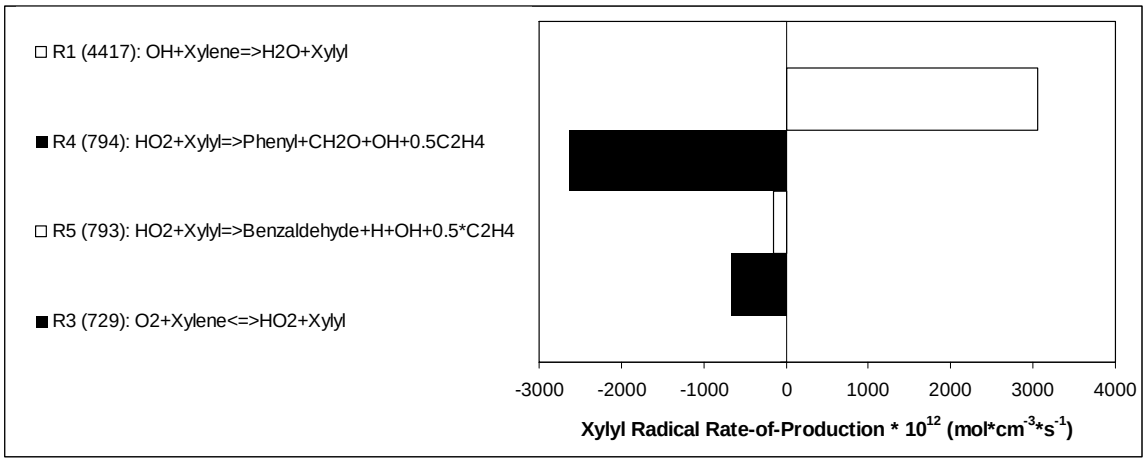

Figure 7-4: Key reactions involving xylyl radical destruction and production.

While the phenyl radical participates in 314 reactions, only six reactions were significant at the 5% level. The ROP for the phenyl radical was -4.95x10^{-14} mol*cm^{-3}*s^{-1}. The main pathway for phenyl radical destruction was via R6 (#742), Fig. 7-5, producing the phenoxy radical (C_6H_5O). Two other pathways important in the conversion of phenyl radical were R7 (#743) and R8 (#734). The main pathway for phenyl radical production was R4, which occurs from the destruction of the xylyl radical. Additional phenyl radical production was through the pathways of R9 (#771) and R10 (#4134).

$$O_2 + C_6H_5 \Leftrightarrow C_6H_5O + O \qquad \text{R6 (742)}$$

$$O_2 + C_6H_5 \Rightarrow C_6H_4O_2 + H \qquad \text{R7 (743)}$$

$$O_2 + C_6H_5 \Rightarrow C_4H_4 + HCO + CO \qquad \text{R8 (734)}$$

$$OH + C_6H_5O \Rightarrow C_6H_5 + HO_2 \qquad \text{R9 (771)}$$

$$OH + C_7H_6O \Rightarrow H_2O + C_6H_5 + CO \qquad \text{R10 (4134)}$$

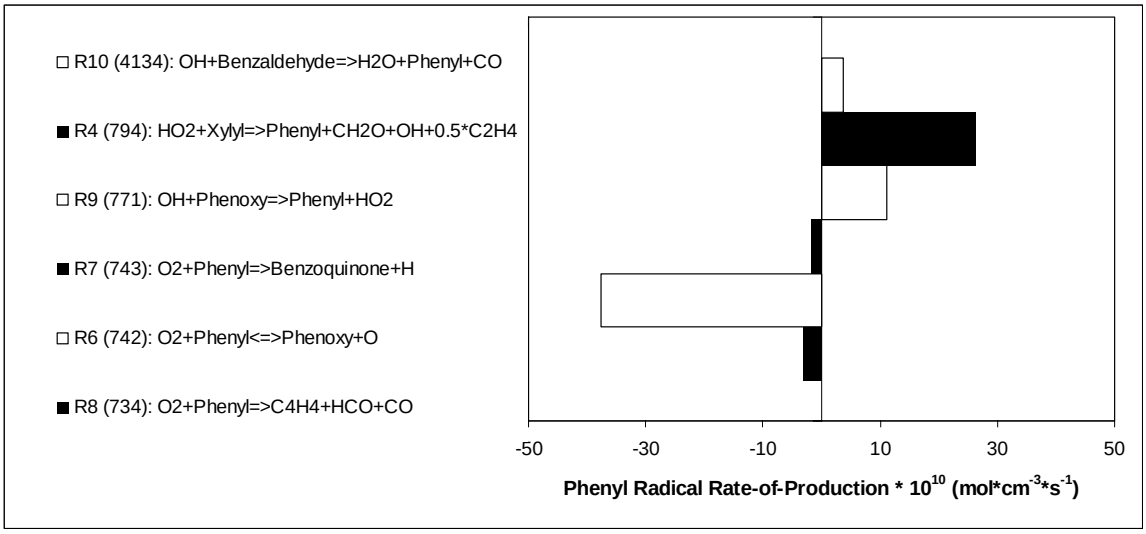

Figure 7-5: Key reactions involving phenyl radical destruction and production.

The ROP for the phenoxy radical was -1.45x10^{-10} mol*cm^{-3}*s^{-1}. Only three of the 50 reactions involving phenoxy radical contributed significantly to its destruction, Figure 7-6. R6 produced a phenyl radical, R11 (#702) reacted to form phenol (C_6H_6O), and R12 (#813) produced cyclopentadiene. As mentioned in the destruction of the phenyl radical, R6 was the main pathway for the production of the phenoxy radical. A minor pathway involved H-atom abstraction from phenol by hydroxyl radical, R13 (#3974).

$$H + C_6H_5O \Leftrightarrow C_6H_6O \qquad \text{R11 (702)}$$

$$H + C_6H_5O \Rightarrow C_5H_6 + CO \qquad \text{R12 (813)}$$

$$OH + C_6H_6O \Rightarrow H_2O + C_6H_5O \qquad \text{R13 (3974)}$$

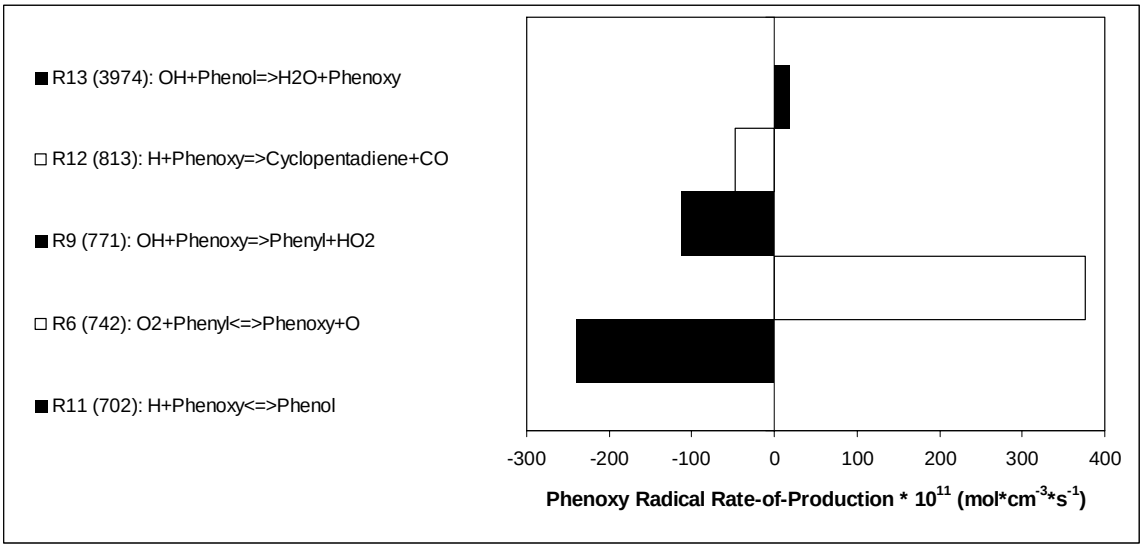

Figure 7-6: Key reactions involving phenoxy radical destruction and production.

Phenol was the final aromatic intermediate identified during the xylene oxidation. Of 49 reactions involving phenol, only two contributed significantly to its total ROP of $2.27x10^{-9}$ mol*cm^{-3}*s^{-1}, Fig. 7-7. As mentioned in the destruction of the phenoxy radical, R11 was the major pathway of phenol production. A minor pathway in consuming phenol was R13, producing the phenoxy radical.

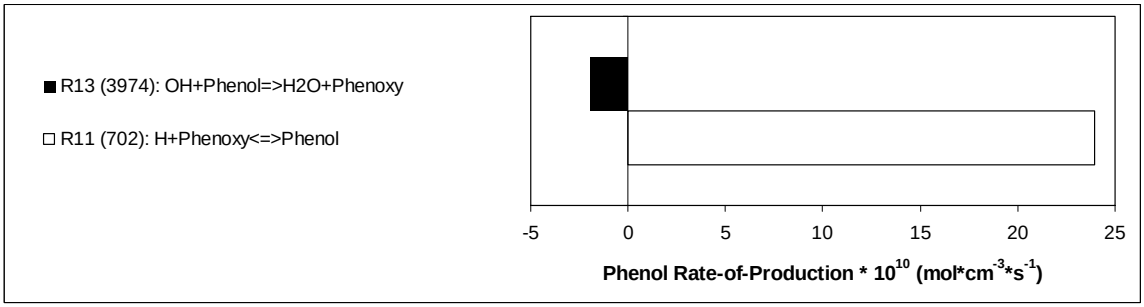

Figure 7-7: Key reactions involving phenol destruction and production.

Based on the analysis of the modeling results, a low temperature branching pathway for xylene oxidation was identified, Fig. 7-8. This pathway traces the parent

fuel to the final stable intermediate identified in the modeling analysis, phenol. Figure 7-8 shows the *m*-xylene and *m*-xylyl isomers, although as modeled this would be applicable for any of the isomers.

The model predicted phenol levels up to 25 ppm, well above the detectability limit of 1 ppm in the MS. Because the model predicted that phenol was the major stable intermediate produced by xylene at these temperatures and no phenol was identified in the PFR experiments, additional testing was conducted to confirm the discrepancy. Phenol was injected into the GC, via the heated sample storage cart, and the GC/MS/FID was operated using the same method as for the PFR experiments (Ch. 5) to ensure that the facility was capable of detecting phenol. The GC/MS/FID successfully identified phenol and thus verified the discrepancy between the model and experiments. Moreover, Lenhert *et al*. (2009) identified phenol as an intermediate from toluene oxidation in the PFR facility. This also removes concern that phenol may have reacted during the quenching process, if it were produced. Therefore, it can be concluded phenol was not produced in the xylene experiments, or else it would have been identified.

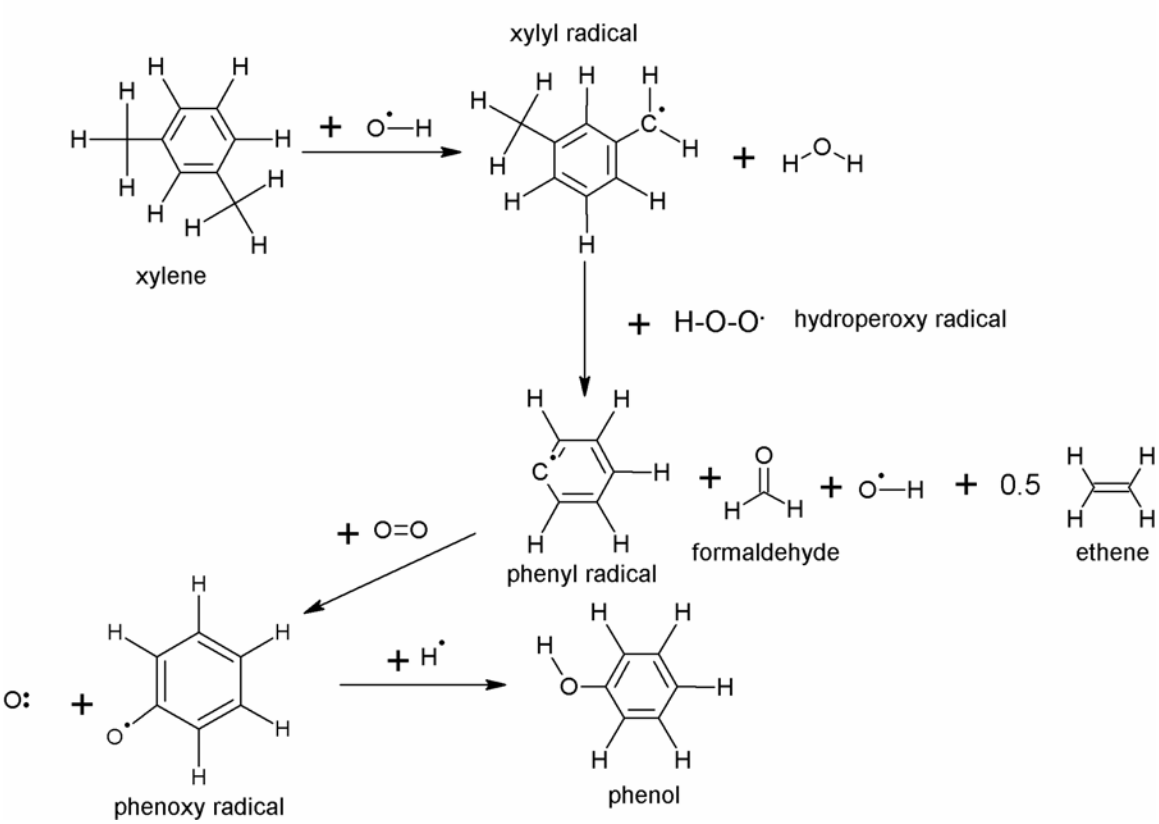

Figure 7-8: Low temperature branching pathway of xylene based on Ranzi *et al.* (2007) model.

To examine possible interactions between the xylene and *n*-dodecane, the small species identified in Figure 7-8 necessary for each reaction pathway – hydroxyl radical, hydroperoxy radical, molecular oxygen, and atomic hydrogen radical – were studied using ROP analysis. In the mechanism, 732 reactions include the hydroxyl radical ($\dot{O}H$). The dominant reaction is R14 (#2481), the production of water and a formyl radical from $\dot{O}H$ and formaldehyde. All reactions with ROP's of at least 20% of this maximum ROP, at 700 K, are shown in Figure 7-9. The ROP was -5.88×10^{-13} mol*cm^{-3}*s^{-1}, indicating that at 700 K $\dot{O}H$ is being consumed faster than it is being produced. While the majority of the dominant reactions involving $\dot{O}H$ are with small species, the

reaction with xylene is also identified as important. The rate-of-production of $\dot{O}H$ thus may limit the reactivity of xylene, as it was identified from Figure 7-3 that $\dot{O}H$ is most likely to attack the xylene molecule. Nevertheless, Figure 7-9 shows that the dominant pathways producing $\dot{O}H$ come from small species, in particular performic acid (CH_2O_3) and methyl peroxide (CH_4O_2), that are produced from the n-dodecane oxidation.

$$OH + CH_2O \Rightarrow H_2O + HCO \qquad \text{R14 (2481)}$$

The hydroperoxy radical was identified as the reactant added to the xylyl radical that produces the phenyl radical. At 700 K, the ROP was -8.11x10^{-10} mol*cm^{-3}*s^{-1} for the hydroperoxy radical. Figure 7-10 shows reactions with ROP values of at least 20% of the maximum ROP for a $H\dot{O}_2$ reaction, indicating that the dominant pathway for the destruction of $H\dot{O}_2$ is the characteristic intermediate temperature pathway of two hydroperoxy radicals reacting to form hydrogen peroxide and O_2. The formation of $H\dot{O}_2$ relied on the reaction of O_2 with the formyl radical.

As shown in Figure 7-8, O_2 reaction with the phenyl radical produces the phenoxy radical. At 700 K, the ROP for O_2 was -6.81x10^{-8} mol*cm^{-3}*s^{-1}. Figure 7-11 shows all reactions with an ROP for O_2 of at least 20% of the maximum. All the reactions involve smaller species, except for the low temperature pathway of the dodecylhydroperoxy n-C_{12}-QOOH reacting with O_2 to form the dihydroperoxide species.

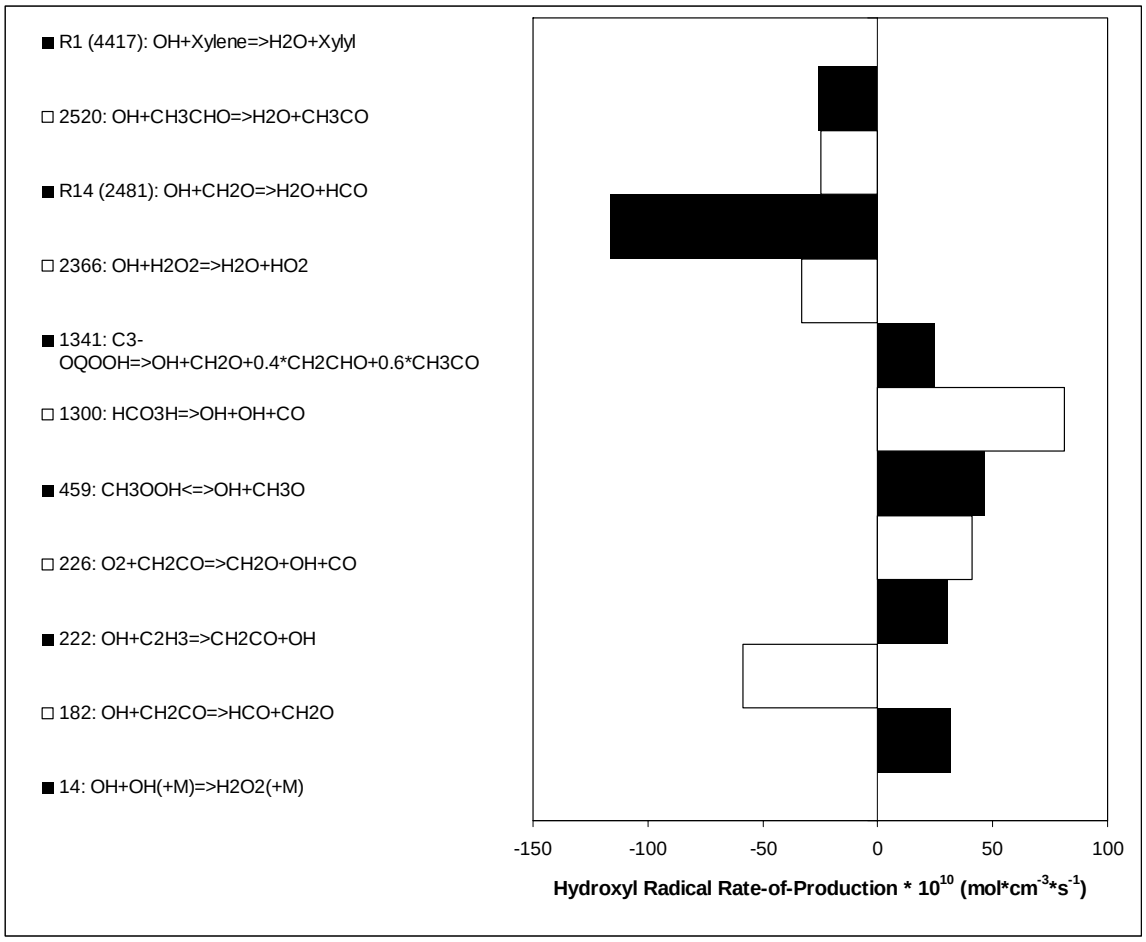

Figure 7-9: Key reactions involving hydroxyl radical destruction and production.

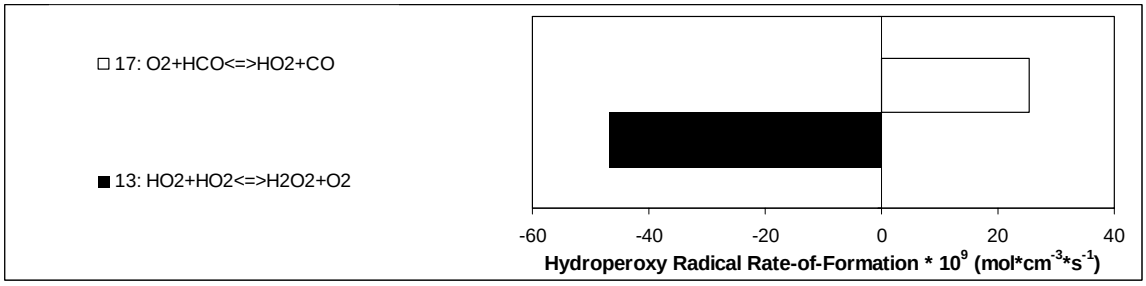

Figure 7-10: Key reactions involving hydroperoxy radical destruction and production.

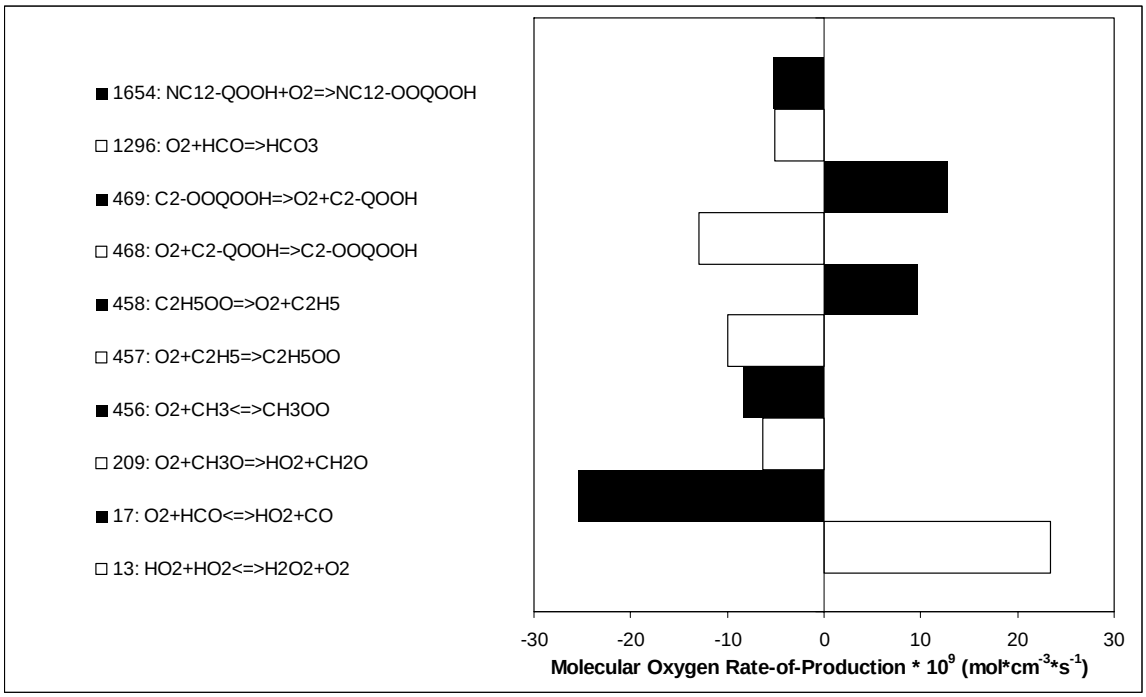

Figure 7-11: Key reactions involving molecular oxygen destruction and production.

The pathway for the phenoxy radical to produce phenol is via $\dot{H}$. Figure 7-12 shows the reactions involving $\dot{H}$ with ROP values of at least 20% of the maximum reaction. At 700 K, the ROP for $\dot{H}$ was -3.01x10^{-12} mol*cm^{-3}*s^{-1}. Interestingly, some competition in consuming $\dot{H}$ may occur. While the reaction of $\dot{H}$ with O_2 to produce the hydroperoxy radical was the dominant reaction, Figure 7-12 also shows that the phenol production pathway also consumed a large fraction of $\dot{H}$.

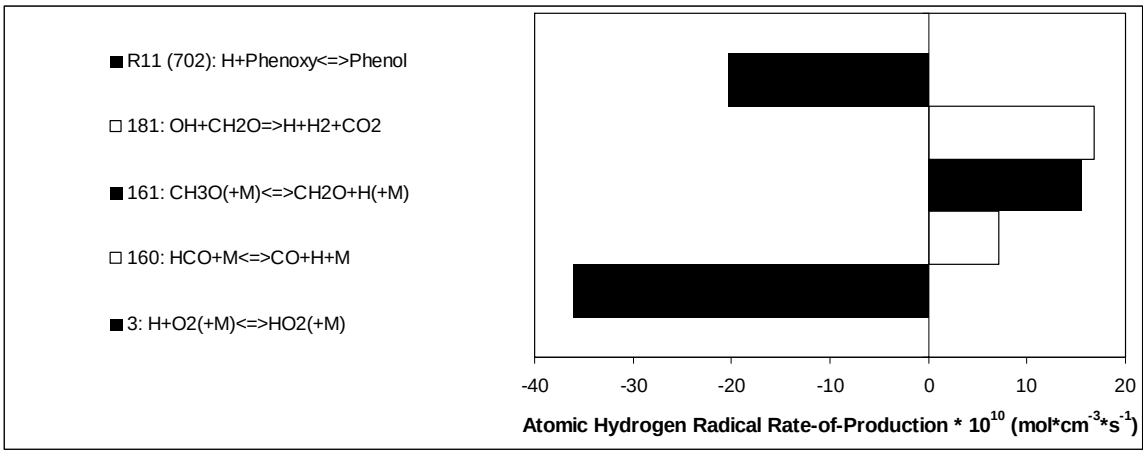

Figure 7-12: Key reactions involving atomic hydrogen destruction and production.

7.2 CNRS Model

The *m*-xylene chemical kinetic model of Gaïl and Dagaut (2007) was evaluated in Chemkin 4.1 at PFR conditions. As explained in Sec. 4.3, only neat *m*-xylene was evaluated. A mixture containing 1200 ppm *m*-xylene (molar fractions of 0.95683 N_2 / 0.04197 O_2 / 0.0012 *m*-C_8H_{10}) showed no reactivity at 700 K temperature, correlating with the neat xylene experiments in the PFR.

7.3 Summary

Two models were compared to the experiments. The significant findings, applicable for lean stoichiometry and in the low temperature regime, are:

(1) The Ranzi *et al*. (2007) and Gaïl and Dagaut (2007) models both predicted no reactivity from neat xylene oxidation,

(2) In binary mixtures with a more reactive component, the Ranzi *et al*. (2007) model accurately predicted the overall reactivity behavior, but the reaction pathways dominant in the model are not those indicated in the experiment, because,

a) the key intermediate predicted by the model was not produced in the experiments, and

b) other species measured experimentally were not predicted from the model.

CHAPTER 8. MECHANISTIC ANALYSIS

8.1 Discussion

The relative reactivity of the xylenes in the PFR and the engine did not agree. In the PFR, the two xylenes tested in mixtures with *n*-dodecane at equivalent conditions (*o*-and *m*-xylene) showed the same reactivity and produced the same intermediate species. However, in the engine, *o*-xylene showed greater reactivity than the other two isomers in mixtures with *n*-decane and in the six-component JP-8 surrogate. An examination of the present reactivity and intermediate speciation results compared to previous xylene studies explains the observations.

Emdee *et al.* (1990 & 1991) identified the major oxidation routes of the xylenes and identified the significance of the pathway to xylylene. Hydrogen abstraction from *o*-xylene produces the *o*-xylyl radical, and reaction with molecular oxygen produces *o*-xylylene. *o*-Xylylene then easily isomerizes to styrene, which can decompose to the reactive species phenyl and vinyl radicals. It is possible that this pathway is not dominant at the temperatures in the PFR (600-850 K), but becomes activated at the higher temperatures in the engine (>1000 K), and thus enables the increased reactivity of *o*-xylene at high temperatures. This is because the structure of the xylylene formed is dependent upon the isomer. Pollack *et al.* (1981) found that *m*-xylylene, the major xylylene species produced by *m*-xylene, has a much higher heat of formation than *o*-xylylene or *p*-xylylene, and thus there is no pathway to rapidly lead to the phenyl and vinyl radicals. For *p*-xylene, Emdee *et al.* (1991) showed that *p*-xylylene is produced, but

the latter leads to other species maintaining the *p*-xylene structure, such as *p*-ethyl-benzaldehyde, rather than the phenyl and vinyl radicals.

At the lower temperatures in the PFR, another pathway for *o*-xylyl radical may be dominant. This scheme is the production of *o*-tolualdehyde and atomic hydrogen radical from the reaction of *o*-xylyl radical with atomic oxygen radical (Emdee *et al.*, 1990). This pathway possibly explains the production of *o*-tolualdehyde in the *n*-dodecane / *o*-xylene PFR experiment. Similar pathways for the production of *m*-tolualdehyde from *m*-xylene and *p*-tolualdehyde from *p*-xylene are also possible.

Another pathway for xylene is the production of toluene. Gaïl and Dagaut (2007) suggested the reaction of *m*-xylene and atomic hydrogen radical to produce toluene and a methyl radical (No. 1182 in their paper), using parameters including a pre-exponential factor (A) of 1.80 x 10^{14} cm^3 / (mol^*K^*s) and an activation energy (E_a) of 8,090 cal/mol. The same reaction for *p*-xylene and *o*-xylene, with the same pre-exponential factor and activation energy, is included in their *p*-xylene and o-xylene models (No. 972 and No. 1361, respectively) (Gaïl and Dagaut, 2005; Gaïl *et al*., 2008). Nevertheless, a competing pathway in the *m*-xylene model is the reaction of *m*-xylene and hydrogen radical to produce *m*-xylyl radical and molecular hydrogen. Gaïl and Dagaut (2007) included this reaction (No. 1177), using an A of 4.00 x 10^{14} cm^3 / (mol^*K^*s) and an E_a of 8,370 cal/mol. Figure 8-1 shows the rate constants (k) for these reactions, indicating both are active at lower temperatures with sufficient quantities of hydrogen radicals. Equivalent reactions for production of the *p*-xylyl and *o*-xylyl radicals can be found in their respective models (No. 964 and No. 1356).

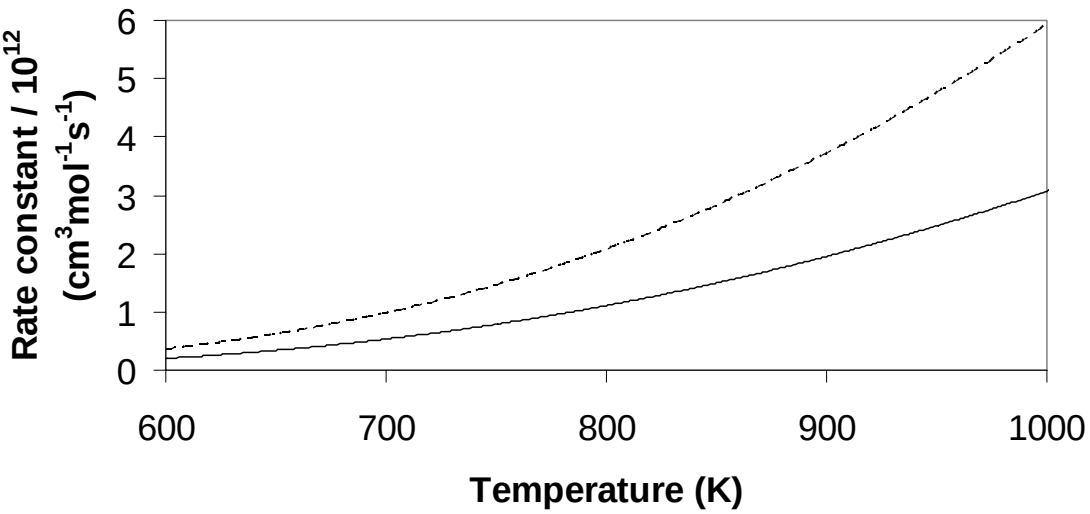

Figure 8-1: Rate constants of reactions No.1182 (—) and No. 1177 (--) from Gaïl and Dagaut (2007).

8.2 Results

Based on the experimental findings and previous high temperature xylene work, general schematics of the low temperature oxidation of the isomers were developed. Figure 8-2 shows the pathways of *o*-xylene oxidation, with the pathway producing 2-methylbenzyl radical (*o*-xylyl radical) and then 2-methylbenzaldehyde (*o*-tolualdehyde) preferred at lower temperatures. At higher temperatures, the *o*-xylyl radical reacts with molecular oxygen to produce 5,6-bis(methylene)cyclohexa-1,3-diene (*o*-xylylene) and hydroperoxy radical. *o*-Xylylene isomerizes to styrene, which decomposes to phenyl and vinyl radicals that promote further reactivity.

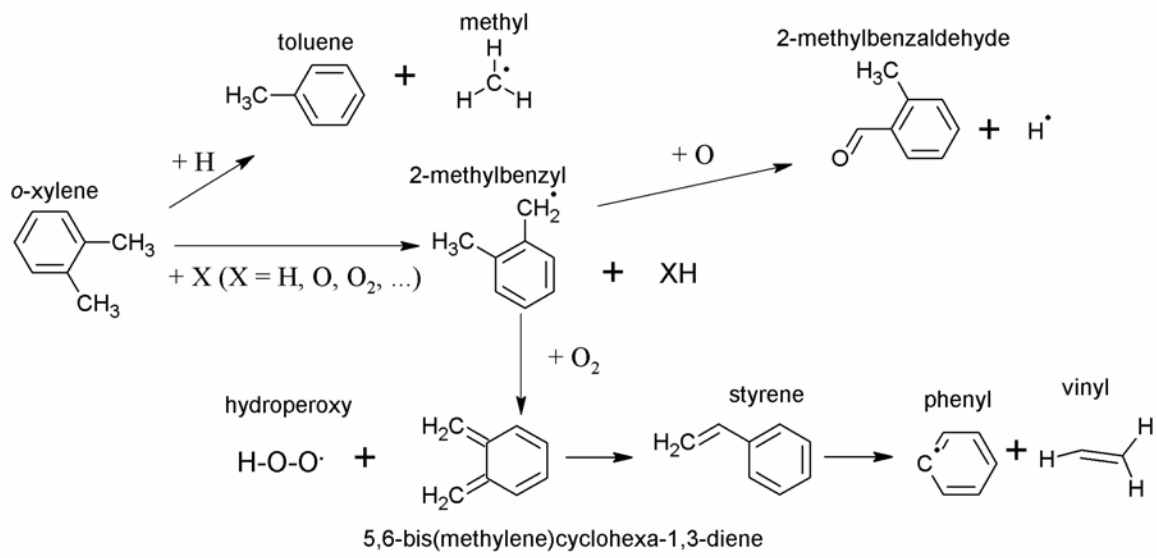

Figure 8-2: Key branching pathways of *o*-xylene oxidation.

Figure 8-3 shows the *m*-xylene oxidation pathways. At lower temperatures, any of several small radicals react with *m*-xylene to form 3-methylbenzyl radical (*m*-xylyl radical) and another species. *m*-Xylyl radical reacts with oxygen radical to form 3-methylbenzaldehyde (*m*-tolualdehyde) and hydrogen radical. Another pathway for *m*-xylene is reaction with hydrogen atom to form toluene and methyl radical. At higher temperatures, *m*-xylyl radical follows different pathways to form species maintaining the *m*-xylene structure.

The oxidation pathways for *p*-xylene are shown in Figure 8-4. At lower temperatures, any of several small species react with *p*-xylene to form 4-methylbenzyl radical (*p*-xylyl radical) and another small species. *p*-Xylyl radical reacts with oxygen radical to form 4-methylbenzaldehyde (*p*-tolualdehyde) and hydrogen radical. Hydroxyl radical attack on *p*-tolualdehyde produces *p*-cresol and formyl radical. Another pathway for *p*-xylene is reaction with hydrogen radical to form toluene and methyl radical. At higher temperatures, *p*-xylyl radical reacts with molecular oxygen to form

3,6-bis(methylene)cyclohexa-1,4-diene (*p*-xylylene) and hydroperoxy radical.

p-Xylylene then forms other species maintaining the *p*-xylene structure.

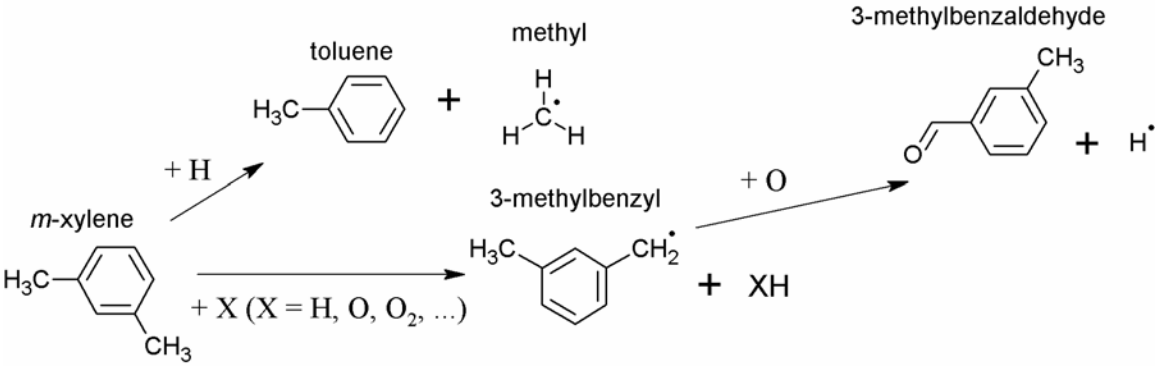

Figure 8-3: Key branching pathways of *m*-xylene oxidation.

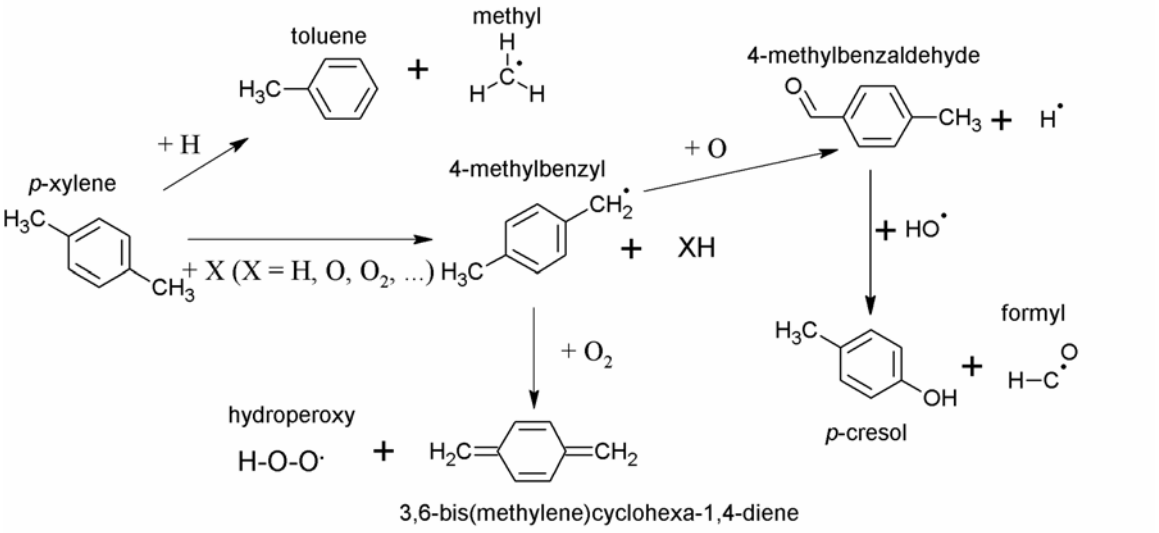

Figure 8-4: Key branching pathways of *p*-xylene oxidation.

CHAPTER 9. CONCLUDING REMARKS

9.1 Summary

The objectives of this study were to determine the relative reactivity of the xylene isomers at preignition and autoignition conditions, and to isolate the key branching pathways of xylene oxidation. At conditions in the PFR, the isomers showed the same reactivity. Their pathways were similar, with each isomer producing its respective tolualdehyde isomer as well as toluene. *p*-Xylene also produced *p*-cresol at low levels, although it must also be acknowledged that the *p*-xylene experiment was conducted at higher fuel concentration compared to the *o*- and *m*-xylene experiments and thus comparison of minor species is not applicable. At autoignition conditions in the engine, *o*-xylene was more reactive than the other isomers. It must be noted that all the PFR and engine experiments were at lean conditions, and the xylenes only exhibited reactivity when in mixtures with alkanes. Neat and at lean conditions, the xylenes were not reactive in the PFR or the engine. These results highlighted the importance in conducting experimental work of surrogate fuel components at low temperatures under conditions relevant for engine combustion (lean equivalence ratios and in mixtures with alkanes). The majority of previous work focused on high temperature combustion of neat xylenes and at stoichiometric conditions. Because of the complex temperature-dependent reaction pathways, the results of those studies cannot be directly translated to low temperature oxidation. Nevertheless, they are helpful, and the previous work provided a background in explaining the present results.

The implications for the findings of this study involve selection of components for surrogate fuels, and the proper manner to study the surrogates. If only preignition

conditions are being considered, selection among the different xylene isomers is inconsequential. However, if conditions at higher temperatures reaching autoignition are important, the reactivity differences among the xylene isomers must be considered. Furthermore, in the continuing development of kinetic models, these experimental results show that lumping of the isomers is acceptable at lower temperatures, but at higher temperatures, the decision of lumping isomers is not as simple, and may depend upon how many species and reactions the model can contain.

9.2 Future Work

The outcome of this work provides several opportunities for future studies. The present study only included identification of intermediates from xylene oxidation in the PFR but not quantification. Quantitative measurements, which are possible because of modifications to the facility after this study, could be conducted. Such experiments would produce a benchmark dataset so that xylene models could be produced and refined based on high quality experimental results. Once more quantitative data are acquired, the present xylene models can be adjusted for predicting low temperature xylene reactivity. For example, the identification of tolualdehyde, toluene, and cresol from xylene oxidation provides a good initial foundation for a low temperature xylene model, but additional quantification experiments would provide information regarding consumption fraction of xylene and conversion rates to the various intermediates.

LIST OF REFERENCES

Agosta, A., 2002, Development of a chemical surrogate for JP-8 aviation fuel using a pressurized flow reactor, M.S. Thesis, Drexel University, Philadelphia, PA.

Agosta, A., Cernansky, N. P., Miller, D. L., Faravelli, T., Ranzi, E., 2004, Reference components of jet fuels: kinetic modeling and experimental results, *Experimental Thermal and Fluid Science 28*:701-708.

Akihama, K., Takatori, Y., Inagaki, K., Sasaki, S., Dean, A. M., 2001, Mechanism of the smokeless rich diesel combustion by reducing temperature, SAE Paper No. 2001-01-0655.

Barnard, J. A., Sankey, B. M., 1968a, The slow combustion of the isomeric xylenes: I: meta- and para-xylene, *Combustion and Flame 12*:345-352.

Barnard, J. A., Sankey, B. M., 1968b, The slow combustion of the isomeric xylenes: II: ortho-xylene, *Combustion and Flame 12*:353-359.

Battin-Leclerc, F., Bounaceur, R., Belmekki, N., Glaude, P.A., 2006, Experimental and modeling study of the oxidation of xylenes, *International Journal of Chemical Kinetics 38*:284-302.

Battin-Leclerc, F., 2008, Detailed chemical kinetic models for the low-temperature combustion of hydrocarbons with application to gasoline and diesel fuel surrogates, *Progress in Energy and Combustion Science 34*:440-498.

Brezinsky, K., 1986, The high-temperature oxidation of aromatic hydrocarbons, *Progress in Energy and Combustion Science 12*:1-24.

Chase, M. W., 1998, NIST-JANAF Thermochemical Tables, Fourth Edition, *Journal of Physical and Chemical Reference Data*, Monograph No. 9.

Colket, M., Edwards, T., Williams, S., Cernansky, N. P., Miller, D. L., Egolfopoulos, F., Lindstedt, P. Seshadri, K., Dryer, F. L., Law, C. K., Friend, D., Lenhert, D. B., Pitsch, H., Sarofim, A., Smooke, M., Tsang, W., 2007, Development of an

experimental database and kinetic models for surrogate jet fuels, *AIAA Paper No. 2007-770.*

Colket, M., Edwards, T., Williams, S., Cernansky, N. P., Miller, D. L., Egolfopoulos, F., Dryer, F. L., Bellan, J., Lindstedt, P., Seshadri, K., Pitsch, H., Sarofim, A., Smooke, M., Tsang, W., 2008, Identification of target validation data for development of surrogate jet fuels, *AIAA Paper No. 2008-0972*.

Dec, J. E., 2009, Advanced compression-ignition engines – understanding the in-cylinder processes, *Proceedings of the Combustion Institute 32*:2727-2742.

Draeger, J. A., 1985, The methylbenzenes. II. Fundamental vibrational shifts, statistical thermodynamic functions, and properties of formation, *Journal of Chemical Thermodynamics 17*:263-275.

Edwards, T., Maurice, L. Q., 2001, Surrogate mixtures to represent complex aviation and rocket fuels, *Journal of Propulsion and Power 17*:461-466.

Edwards, T. (Wright-Patterson Air Force Base), 2003, Personal communication.

Emdee, J. L., Brezinsky, K., Glassman, I., 1990, Oxidation of o-xylene, *Proceedings of the Combustion Institute 23*: 77-84.

Emdee, J. L., Brezinsky, K., Glassman, I., 1991, High temperature oxidation mechanisms of m- and p-xylene, *Journal of Physical Chemistry 95*:1626-1635.

Eng, R. A., Fittschen, C., Gebert, A., Hibomvschi, P., Hippler, H., Unterreiner, A.-N., 1998, Kinetic investigations of the reactions of toluene and of p-xylene with molecular oxygen between 1050 and 1440 K, *Proceedings of the Combustion Institute 27*:211-218.

Farrell, J. T., Cernansky, N. P., Dryer, F. L., Friend, D. G., Hergart, C. A., Law, C. K., McDavid, R. M., Mueller, C. J., Patel, A. K., Pitsch, H., 2007, Development of an experimental database and kinetic models for surrogate diesel fuels, *SAE Paper No. 2007-01-0201*.

Ferguson, C. R., Kirkpatrick, A. T., 2001, *Internal Combustion Engines*, Second Edition, John Wiley & Sons, Inc., New York, NY.

Gaïl, S., Dagaut, P., 2005, Experimental kinetic study of the oxidation of p-xylene in a JSR and comprehensive detailed chemical kinetic modeling, *Combustion and Flame 141*: 281-297.

Gaïl, S., Dagaut, P., 2007, Oxidation of m-xylene in a JSR: experimental study and detailed chemical kinetic modeling, *Combustion Science and Technology 179*:813-844.

Gaïl, S., Dagaut, P., Black, G., Simmie, J. M., 2008, Kinetics of 1,2-dimethylbenzene oxidation and ignition: experimental and detailed chemical kinetic modeling, *Combustion Science and Technology 180*:1748-1771.

Gong, X., 2005, The effects of DTBP on the oxidation of SI primary reference fuels – a study in an HCCI engine and in a pressurized flow reactor, Ph.D. Thesis, Drexel University, Philadelphia, PA.

Gregory, D., Jackson, R. A., Bennett, P. J., 1999, Mechanisms for the formation of exhaust hydrocarbons in a single-cylinder spark ignition engine, fueled with deuterium-labeled ortho-, meta-, and para-xylene, *Combustion and Flame 118*:459-468.

Griffiths, J. F., 1995, Reduced kinetic models and their application to practical combustion systems, *Progress in Energy and Combustion Science 21*:25-107.

Guibet, J. C., 1999, *Fuels and Engines: Technology, Energy, Environment*, Revised Edition, Institut Francais du Petrole Publications, Paris, France.

Holley, A. T., Dong, Y., Andac, M. G., Egolfopoulos, F. N., Edwards, T., 2007, Ignition and extinction of non-premixed flames of single-component liquid hydrocarbons, jet fuels, and their surrogates, *Proceedings of the Combustion Institute 31*:1205-1213.

Jackson, J. L., 1951, Spontaneous ignition temperatures, *Industrial and Engineering Chemistry 43*:2869-2870.

Jet Fuel Surrogate Working Group Meeting, 2008, Reno, NV, January 6.

Johnson, R., Natelson, R., Kurman, M., Miller, D. L., Cernansky, N.P., 2005, The auto-ignition of JP-8, Jet A, and Selected Fuel Components in a Single Cylinder Engine, Fall Meeting of the Western States Section of the Combustion Institute, Paper No. WSSCI-05F-55, Stanford, CA.

Johnson, R. O., 2007, A fundamental study of the autoignition behavior of SI primary reference fuels with propionaldehyde and DTBP as an additive, M.S. Thesis, Drexel University, Philadelphia, PA.

Kee, R. J., Rupley, F. M., Miller, J. A., Coltrin, M. E., Grcar, J. F., Meeks, E., Moffat, H. K., Lutz, A. E., Dixon-Lewis, G., Smooke, M. D., Warnatz, J., Evans, G. H., Larson, R. S., Mitchell, R. E., Petzold, L. R., Reynolds, W. C., Caracotsios, M., Stewart, W. E., Glarborg, P., Wang, C., McLellan, C. L., Adigun, O., Houf, W. G., Chou, C. P., Miller, S. F., Ho, P., Young, P. D., Young, D. J., Hodgson, D. W., Petrova, M. V., Puduppakkam, K. V., 2006, CHEMKIN Release 4.1, Reaction Design, San Diego, CA.

Koert, D. N., 1990, Effects of pressure on hydrocarbon oxidation chemistry, Ph.D. Thesis, Drexel University, Philadelphia, PA.

Koert, D. N., Cernansky, N. P., 1992, A flow reactor for the study of homogeneous gas-phase oxidation of hydrocarbons at pressures up to 20 atm (2 MPa), *Measurement Science and Technology 3*:607-612.

Kurman, M. S., 2009, The preignition and autoignition oxidation of alternatives to petroleum derived JP-8 and their surrogate components in a pressurized flow reactor and single cylinder research engine, M.S. Thesis, Drexel University, Philadelphia, PA.

Kurman, M. S., Natelson, R. H., Cernansky, N. P., Miller, D. L., 2009a, Preignition oxidation chemistry of the major JP-8 surrogate component: n-dodecane, *AIAA Paper No. 2009-1526*.

Kurman, M. S., Natelson, R. H., Cernansky, N. P., Miller, D. L., 2009b, New methodology for jet fuel surrogate oxidation and intermediate speciation in the low

temperature regime, 6th U.S. National Combustion Meeting, Paper No. USSCI-09-23G2, Ann Arbor, MI.

Law, C. K., 2006, *Combustion Physics*, Cambridge University Press, New York, NY.

Lenhert, D. B., 2004a, The oxidation of JP-8 and its surrogates in the low and intermediate temperature regime, Ph.D. Thesis, Drexel University, Philadelphia, PA.

Lenhert, D. B., 2004b, The oxidation of a gasoline fuel surrogate in the negative temperature coefficient region, M.S. Thesis, Drexel University, Philadelphia, PA.

Lenhert, D. B., Miller, D. L., Cernansky, N. P., 2007, The oxidation of JP-8, Jet-A, and their surrogates in the low and intermediate temperature regime, *Combustion Science and Technology 179*:845-861.

Lenhert, D. B., Miller, D. L., Cernansky, N. P., Owens, K. G., 2009, The oxidation of a gasoline surrogate in the negative temperature coefficient region, *Combustion and Flame 156*:549-564.

Loftus, J., Satterfield, C. N., 1965, Mechanism of homogeneous gas-phase partial oxidation of o-xylene, *Journal of Physical Chemistry 69*:909-918.

Lovell, W. G., Campbell, J. M., Boyd, T. A., 1934, Knocking characteristics of hydrocarbons determined from compression ratios at which individual compounds begin to knock under specified conditions, *Industrial and Engineering Chemistry 26*:1105-1108.

McEnally, C. S., Pfefferle, L. D., Atakan, B., Kohse-Höinghaus, K., 2006, Studies of aromatic hydrocarbon formation mechanisms in flames: progress towards closing the fuel gap, *Progress in Energy and Combustion Science 32*:247-294.

Miller, J. A., Pilling, M. J., Troe, J., 2005, Unravelling combustion mechanisms through a quantitative understanding of elementary reactions, *Proceedings of the Combustion Institute 30*:43-88.

Natelson, R. H., Kurman, M. S., Cernansky, N. P., Miller, D. L., 2008, Experimental investigation of surrogates for jet and diesel fuels, *Fuel 87*:2339-2342.

Pollack, S. K., Raine, B. C., Hehre, W. J., 1981, Determination of the heats of formation of the isomeric xylylenes by ion cyclotron double-resonance spectroscopy, *Journal of the American Chemical Society 103*:6308-6313.

Ramotowski, M. J., 1992, The oxidation of propane and n-butane at elevated pressures in the region of negative temperature coefficient, M.S. Thesis, Drexel University, Philadelphia, PA.

Ranzi, E., Frassoldati, A., Granata, S., Faravelli, T., 2005, Wide-range kinetic modeling study of the pyrolysis, partial oxidation, and combustion of heavy n-alkanes, *Industrial and Engineering Chemistry Research 44*:5170-5183.

Ranzi, E., Faravelli, T., Frassoldati, A., 2007, CRECK Modeling, Milano, Italy, August 3, available at http://www.chem.polimi.it/creckmodeling/.

Reaction Design, 2007a, CHEMKIN Software Input Manual, San Diego, CA.

Reaction Design, 2007b, CHEMKIN Theory Manual, San Diego, CA.

Richter, H., Howard, J. B., 2000, Formation of polycyclic aromatic hydrocarbons and their growth to soot – a review of chemical reaction pathways, *Progress in Energy and Combustion Science 26*:565-608.

Roubaud, A., Minetti, R., Sochet, L. R., 2000a, Oxidation and combustion of low alkylbenzenes at high pressure: comparative reactivity and auto-ignition, *Combustion and Flame 121*:535-541.

Roubaud, A., Lemaire, O., Minetti, R., Sochet, L. R., 2000b, High-pressure auto-ignition and oxidation mechanisms of o-xylene, o-ethyltoluene, and n-butylbenzene between 600 and 900 K, *Combustion and Flame 123*:561-571.

Pitz, W. J., Cernansky, N. P., Dryer, F. L., Egolfopoulos, F. N., Farrell, J. T., Friend, D. G., Pitsch, H., 2007, Development of an experimental database and chemical kinetic models for surrogate gasoline fuels, *SAE Paper No. 2007-01-0175*.

Scott, D. W., 1974, Correlation of the chemical thermodynamic properties of alkane hydrocarbons, *Journal of Chemical Physics 60*:3144-3165.

Semenov, N. N., 1935, *Chemical Kinetics and Chain Reactions*, Oxford University Press, London.

Seshadri, K., 2006, Autoignition and combustion of diesel and JP-8, ARO/AFOSR Contractors' Meeting on Chemical Propulsion, Arlington, VA.

Simmie, J. M., 2003, Detailed chemical kinetic models for the combustion of hydrocarbon fuels, *Progress in Energy and Combustion Science 29*:599-634.

Smith, B. L., Bruno, T. J., 2007, Composition-explicit distillation curves of aviation fuel JP-8 and a coal-based jet fuel, *Energy and Fuels 21*:2853-2862.

Sjöberg, M., Dec, J. E., 2007, Comparing late-cycle autoignition stability for single- and two-stage ignition fuels in HCCI engines, *Proceedings of the Combustion Institute 31*:2895-2902.

U. S. Army Tank-Automotive and Armaments Command (TACOM), 2001, *JP-8: The Single Fuel Forward: An Information Compendium*, Warren, MI.

Violi, A., Yan, S., Eddings, E. G., Sarofim, A. F., Granata, S., Faravelli, T., Ranzi, E., 2002, Experimental formulation and kinetic model for JP-8 surrogate mixtures, *Combustion Science and Technology 174*:399-417.

Wang, S., 1999, Experimental and modeling study of preignition chemistry of hydrocarbons, Ph.D. Thesis, Drexel University, Philadelphia, PA.

Westbrook, C. K., Dryer, F. L., 1984, Chemical kinetic modeling of hydrocarbon combustion, *Progress in Energy and Combustion Science 10*:1-57.

Wilk, R. D., Koert, D. N., Cernansky, N. P., 1989, Low-temperature carbon monoxide formation as a means of assessing the autoignition tendency of hydrocarbons and hydrocarbon blends, *Energy and Fuels 3*:292-298.

Wright, F. J., 1960, Gas phase oxidation of the xylenes: general kinetics, *Journal of Physical Chemistry 64*:1944-1950.